AIAA JOURNAL
Vol. 57, No. 12, December 2019

Variable-Fidelity Lower Confidence Bounding Approach for Engineering Optimization Problems with Expensive Simulations

Ping Jiang,* Ji Cheng,† Qi Zhou,‡ Leshi Shu,§ and Jiexiang Hu§
Huazhong University of Science & Technology, 430074 Wuhan, People's Republic of China

DOI: 10.2514/1.J058283

Engineering design optimization with expensive simulations is usually a computationally prohibitive process. As one of the most famous efficient global optimization approaches, the lower confidence bounding (LCB) approach has been widely applied to relieve this computational burden. However, the LCB approach can be used only for design optimization problems with the single-fidelity level. In this paper, a variable-fidelity lower confidence bounding (VF-LCB) approach is developed to extend the LCB approach to engineering problems with multifidelity levels. First, a VF-LCB function is analytically derived to adaptively select LF or HF samples according to the predicted values and uncertainty from the VF metamodel. Then the coefficient of variations (CoV) of the predicted values and uncertainty of the VF model, which can reflect the degree of dispersion of the prediction values and uncertainty, respectively, are introduced to balance the global exploration and local exploitation objectively. To illustrate the effectiveness and merits of the proposed VF-LCB approach, eight numerical examples, and the design of micro-aerial vehicle (MAV) fuselage are tested. Comparative results between the proposed approach and the other five existing methods show that the average cost savings are about 25% for eight numerical examples and about 45% for the MAV problem compared with the other five existing methods.

Nomenclature

b	=	weighting parameter in lower confidence bounding function
$\boldsymbol{C}$	=	discrepancy function of variable-fidelity metamodel
c	=	cost ratio between the high-fidelity and low-fidelity models
f	=	actual response at sample
$\hat{f}$	=	predictor function of the kriging model
$\boldsymbol{f}$	=	column vector of responses at sample points
G	=	prediction for constraints
N	=	number of sample points
p	=	column vector filled with ones
$\boldsymbol{R}$	=	correlation matrix in the kriging model
$\boldsymbol{R}(x_i, x_j)$	=	correlation function between points x_i and x_j
$\boldsymbol{r}$	=	correlation vector
s	=	estimated standard error
t	=	fidelity level
W	=	number of iteration
$\boldsymbol{x}$	=	design vector
y	=	actual global optimum
$\hat{y}$	=	estimated objective function
Z	=	Gaussian stochastic process with zero mean and nonzero covariance
β	=	constant term of the kriging model
$\hat{\beta}$	=	estimation of β
γ	=	relaxation factor
ε	=	absolute error between predicted optimum and the actual optimum
σ	=	variance
CoV_f	=	coefficient of variations of prediction
CoV_rmse	=	coefficient of variations of the model's uncertainty

Subscripts

f	=	prediction value
h	=	quantities associated with high fidelity
i, j	=	free indices for elements in a vector or matrix
l	=	quantities associated with high fidelity
m_h	=	number of high-fidelity sample points
m_l	=	number of low-fidelity sample points
n	=	number of iteration
vf	=	quantities associated with variable fidelity
rmse	=	root mean square errors

I. Introduction

METAMODELS (or surrogate models) are widely used in engineering design optimization problems to replace the computational simulation models, aiming to relieve the computational burden [1–4]. There are several commonly used metamodels, such as polynomial response surface (PRS) models [5,6], radial basis function (RBF) models [7,8], kriging models [9,10], support vector regression (SVR) models [11,12], and artificial neural networks (ANN) models [13,14]. Generally, in metamodel-based design and optimization (MBDO), the quantity of interest (QOI) at the sample points can always be obtained by different fidelity computational simulation models. A high-fidelity (HF) analysis model can mimic the QOI accurately and give detailed information of the QOI, but it leads to the dramatic increase of the computational cost. Low-fidelity (LF) analytical model can significantly reduce the cost and keeps the prominent characteristics of the system, but it may result in an inaccurate surrogate model or even a distorted one. Hence, it seems that conflict between the high accuracy of a metamodel and low expenses of analysis is inevitable in the construction of metamodels [15].

To resolve this conflict, variable-fidelity (VF) metamodeling approaches based on the interaction of data from both HF and LF models have grown in popularity in engineering design optimization [16–18]. The VF metamodel can integrate the advantages of LF and HF models, that is, reducing the computational cost while guaranteeing the prediction accuracy of metamodel [19]. There are three main methods to construct a VF metamodel: the scaling-function-based VF metamodeling, the space-mapping approach, and

Received 15 January 2019; revision received 27 June 2019; accepted for publication 23 July 2019; published online 23 August 2019.

*Professor, The State Key Laboratory of Digital Manufacturing Equipment and Technology, School of Mechanical Science and Engineering.

†Graduate Student, The State Key Laboratory of Digital Manufacturing Equipment and Technology, School of Mechanical Science and Engineering.

‡Assistant Professor, School of Aerospace Engineering; qizhouhust@gmail.com (Corresponding Author).

§Ph.D. Candidate, The State Key Laboratory of Digital Manufacturing Equipment and Technology, School of Mechanical Science and Engineering.

the VF kriging. The scaling-function-based VF metamodeling can be divided into three distinct types [20]. The first scaling type is the multiplicative scaling approach, which employs a scaling function to depict the ratio between the HF and LF models [21]. The second one is the additive scaling approach, in which a scaling function is used to capture the differences between the HF and LF models [22]. Lastly, a hybrid scaling approach combines the advantages of the multiplicative and additive scaling approaches to construct the scaling function [20,23]. The space-mapping method constructs a VF metamodel by mapping the parameter space of the HF model to that of the LF one [24,25]. The third method is to construct VF metamodel by co-kriging or its extensions [26]. The co-kriging was originated from the geostatistics community and then extended to integrate the different fidelity levels in the deterministic computational experiments by Kennedy and O'Hagan [27], in which the sum of a scaled LF response and a discrepancy function was adopted to approximate the HF function. There are many extensions for co-kriging, for example, Hierarchical kriging (HK) proposed by Han and Görtz [28], in which the LF kriging model is directly taken as the model trend of the HF kriging.

The quality of a metamodel is mainly dependent on the sample points, and it directly influences the quality of the MBDO. Generally, too few sample points result in a metamodel with poor accuracy, which may affect subsequent optimization process and result in a poor solution. While oversampling is a waste of computational resources, especially the simulation model is computationally expensive [29,30]. To address this issue, the most popular sequential sampling criterion, efficient global optimization (EGO) algorithm, was developed by Jones et al. [31], in which an expected improvement (EI) function was proposed to make a trade-off between global exploration and local exploitation. Cox and John [32] developed a statistical function, named "lower confidence bounding" (LCB), in which a linear combination of the predicted values and the uncertainty is introduced. Furthermore, many enhancement works have been done on these two EGO algorithms [33–35]. For example, Qin et al. [36] provided rigorous insight into EI and introduced a simple modification of the EI algorithm to overcome the best-arm identification problem. Zheng et al. [37] proposed a parameterized LCB approach, in which a cooling strategy is introduced to guarantee the balance between exploitation and exploration by varying weights of the prediction error and the prediction value. Although the previous work demonstrated the obvious merits of EI and LCB algorithms, for the computationally expensive HF models, even performing the number of simulations needed for constructing a metamodel could be too expensive [35,38,39]. To further alleviate the high computational cost in HF analyses, Huang et al. [40] proposed a kriging-based sequential optimization using multifidelity evaluations. Xiong et al. [41] developed a VF optimization approach, which employed the statistical lower bounding criterion as the sequential sampling strategy. Recently, Zhang et al. [42] developed a variable-fidelity EI method assisted with HK, which can adaptively select new samples of both LF and HF. Liu et al. [43] proposed an enhanced co-kriging-based sequential optimization method, which considered the full correlation of data among all multifidelity and extended EI function to reduce computational cost. Notice that these VF methods are mainly developed according to the EI sampling criterion. Compared with the EI sampling criterion, the LCB criterion provides a more intuitive concept and natural implementation process. However, the LCB method cannot be directly used when variable fidelity models are available. Therefore, extending the single-fidelity LCB approach to engineering problems with multifidelity levels is required.

To fill in this gap, a variable-fidelity lower confidence bounding (VF-LCB) approach is proposed. In the proposed approach, a VF-LCB function is derived, which extends the single-fidelity LCB function to adaptively determinate both location and fidelity level of the samples in the process of MBDO. Besides, the coefficient of variations (CoV) of the predicted values and uncertainty of the VF metamodel, which can reflect the degree of dispersion of the prediction values and uncertainty, respectively, are introduced to balance the global exploration and local exploitation objectively. The performance of the proposed VF-LCB approach is illustrated using eight analytical examples and one real-world engineering example. The comparisons between the proposed approach and some existing approaches considering the computational efficiency and robustness are made. The merits of the proposed approach are analyzed and summarized.

The remainder of this paper is organized as follows. The second part recalls the theoretical knowledge of the kriging model and VF metamodeling methods. Then, in Sec. III, the proposed VF-LCB method is introduced in detail. In Sec. IV, an illustrative case is employed to demonstrate the detailed process of the VF-LCB approach, and then eight numerical examples and the design of micro-aerial vehicle (MAV) fuselage are selected to verify the effectiveness of the proposed method. Finally, conclusions are provided in Sec. V.

II. Background

A. Kriging Model

Kriging is an interpolative Bayesian metamodeling technique. It originated in the geostatistical community and then was used to approximate black-box functions by treating the observed response as a combination of a global model and local deviations [44]. The kriging model can be expressed as,

$$\hat{f}(\boldsymbol{x}) = p(\boldsymbol{x}) + Z(\boldsymbol{x}) \tag{1}$$

where $p(\boldsymbol{x})$ is a known polynomial function, and $Z(\boldsymbol{x})$ is a Gaussian stochastic process with zero mean and nonzero covariance.

The covariance of $Z(\boldsymbol{x})$ is formulated as,

$$\mathrm{COV}(Z(x_i), Z(x_j)) = \sigma^2 \boldsymbol{R}(x_i, x_j) \tag{2}$$

where σ^2 is the variance of $Z(\boldsymbol{x})$. $\boldsymbol{R}(x_i, x_j)$ is the correlation function between points x_i and x_j, and it can be expressed as,

$$\boldsymbol{R}(x_i, x_j) = \exp\left[-\sum_{q=1}^{d} \theta_q (x_i^q - x_j^q)^2\right] \tag{3}$$

where d is the dimension of the design variables, and θ_q is a "roughness" parameter associated with the dimension q.

The kriging model has zero mean square error (MSE) at all the observed points because it is an interpolative metamodeling technique. The predictor at an unobserved point can be expressed as,

$$\hat{f}(x) = \boldsymbol{h}^T(x)\hat{\beta} + \boldsymbol{r}^{\boldsymbol{T}}(x)\boldsymbol{R}^{-1}(\boldsymbol{f} - \hat{\beta}\boldsymbol{p}) \tag{4}$$

where $\hat{f}(x)$ is the estimated value of the actual response $f(x)$, and $\boldsymbol{h}(x) = [h_1(x), h_2(x), \ldots, h_N(x)]$ is a vector of regression functions. $\boldsymbol{R}$ is the correlation matrix whose elements are correlation functions between sample points, $\boldsymbol{p}$ is a column vector filled with ones if $p(\boldsymbol{x})$ is taken as a constant, $\boldsymbol{f}$ is the column vector that contains the responses at the sample points, and $\boldsymbol{r}^{\boldsymbol{T}}(x)$ is a correlation vector between the unobserved point and the sample points,

$$\boldsymbol{r}^{\boldsymbol{T}}(x) = [R(x, x_1), R(x, x_2), \ldots, R(x, x_N)]^T \tag{5}$$

where N is the number of sample points.

To compute Eq. (4), there are a number of hyperparameters to be estimated, including $\hat{\beta}$, $\hat{\sigma}$, and θ_q, for $q = 1, 2, \ldots, d$. The hyperparameters are estimated by maximizing the natural logarithm likelihood function, which is given as,

$$-\frac{n}{2}\log(2\pi) - \frac{n}{2}\log(\sigma^2) - \frac{1}{2}\log(|\boldsymbol{R}|) - \frac{(f - \boldsymbol{p}^T\beta)^T\boldsymbol{R}^{-1}(f - \boldsymbol{p}^T\beta)}{2\sigma^2} \tag{6}$$

By taking derivatives of Eq. (6) and setting it to be zero, the maximum likelihood estimates for $\hat{\beta}$ and $\hat{\sigma}^2$ can be obtained as,

$$\hat{\beta} = (\boldsymbol{p}^T \boldsymbol{R}^{-1} \boldsymbol{p})^{-1} \boldsymbol{R}^{-1} \boldsymbol{p}^T \boldsymbol{f}, \quad \hat{\sigma}^2 = \frac{(\boldsymbol{f} - \hat{\beta}\boldsymbol{p})^T \boldsymbol{R}^{-1} (\boldsymbol{f} - \hat{\beta}\boldsymbol{p})}{N} \tag{7}$$

B. Variable-Fidelity Metamodeling

VF metamodel is constructed by integrating the data from HF and LF models to approximate the original system. In the VF metamodel, it is generally considered that there is a difference between the responses obtained by the HF and LF models, but the overall trend of their output responses remains the same [45]. There are usually four ways to simplify the HF model to obtain an LF model [28,46–49]: 1) Simplify the mathematical description of the physical model; for example, the viscous Navier–Stokes equation model can be reduced to a nonviscous Euler equation model. 2) Reduce the dimensionality of the physical model; for example, the low-dimensional model corresponding to the high-dimensional model is used. 3) Change the degree of discretization of the model; for example, a coarse finite element mesh is used instead of the refined finite element mesh. 4) Simplify the way to obtain the performance responses, for example, using a simplified physical experiment to obtain the responses. In the VF metamodeling process, the LF model is used to reduce the computational cost, whereas the HF model is employed to calibrate the LF model and guarantee accuracy.

The scaling-function-based approach is the most commonly used method for constructing a VF metamodel, in which three scaling function types are generally adopted, that is, multiplicative scaling function, additive scaling function, and hybrid scaling function. Among these scaling function types, the additive scaling approach has been widely used in engineering design problems because of its clear concept and simple calculation. In this study, the additive scaling approach is selected to build the VF model. The scaling process is briefly introduced below.

For a given LF sample set $\boldsymbol{x}_l = \{\boldsymbol{x}_1^l, \boldsymbol{x}_2^l, \ldots, \boldsymbol{x}_{m_l}^l\}$ and the corresponding responses $\boldsymbol{f}_l = \{f_1^l, f_2^l, \ldots, f_{m_l}^l\}$, an LF metamodel can be constructed using the kriging model. For the HF sample set $\boldsymbol{x}_h = \{\boldsymbol{x}_1^h, \boldsymbol{x}_2^h, \ldots, \boldsymbol{x}_{m_h}^h\}$ and the corresponding responses $\boldsymbol{f}_h = \{f_1^h, f_2^h, \ldots, f_{m_h}^h\}$, the discrepancies $\boldsymbol{C}(\boldsymbol{x}) = \{c(\boldsymbol{x}_1^h), c(\boldsymbol{x}_2^h), \ldots, c(\boldsymbol{x}_{m_h}^h)\}$ at a HF sample point $\boldsymbol{x}_i^h$ between the LF metamodel and HF model can be expressed as,

$$c(\boldsymbol{x}_i^h) = f_i^h - \hat{f}_l(\boldsymbol{x}_i^h) \tag{8}$$

where f_i^h is the actual response at the point $\boldsymbol{x}_i^h$, and $\hat{f}_l(\boldsymbol{x}_i^h)$ is the predicted value of the LF metamodel for $\boldsymbol{x}_i^h$.

The scaling function $\boldsymbol{C}(\boldsymbol{x})$ can be modeled based on the HF sample set $\boldsymbol{x}_h$ and corresponding scaling data $\boldsymbol{C}(\boldsymbol{x})$ using the kriging model,

$$\hat{\boldsymbol{C}}(\boldsymbol{x}) = \hat{\beta}_h + \boldsymbol{r}_h^T(\boldsymbol{x}) \boldsymbol{R}_h^{-1} (\boldsymbol{f}_h(\boldsymbol{x}) - \hat{\boldsymbol{f}}_l(\boldsymbol{x}) - \hat{\beta}_h \boldsymbol{p}) \tag{9}$$

After the construction of the LF metamodel and scaling function, the VF metamodel can be expressed as,

$$\hat{\boldsymbol{f}}_{\text{vf}}(\boldsymbol{x}) = \hat{\boldsymbol{f}}_l(\boldsymbol{x}) + \hat{\boldsymbol{C}}(\boldsymbol{x}) \tag{10}$$

The uncertainty of the VF metamodel prediction is calculated by

$$\sigma_{\text{vf}}(\boldsymbol{x}) = \sqrt{\sigma_l^2(\boldsymbol{x}) + \sigma_C^2(\boldsymbol{x})} \tag{11}$$

where $\sigma_l(\boldsymbol{x})$ and $\sigma_C(\boldsymbol{x})$ represent the uncertainty of the LF metamodel and scaling function, respectively.

III. Proposed Approach

The goal of the proposed VF-LCB approach is to obtain an accurate-enough optimum while reducing the computational cost by integrating the information from both LF and HF models. In the VF-LCB approach, an LF metamodel is built first. Then, a VF metamodel is constructed by mapping the LF model to the studied HF model using an additive scaling function. If the required accuracy of the optimal solution is not achieved, the proposed approach enters into the iterative optimization process. In the iterative optimization process, the computational resources are adaptively allocated to the HF or LF models according to the already obtained information. Besides, the statistical information, CoV, is employed to improve the weighting in the original LCB function to make a trade-off between a search for the optimum and a search for unexplored regions, instead of subjectively setting the weighting parameters by experiments or experience. The outline of the proposed approach is provided in Fig. 1, and the step-by-step descriptions are depicted in Sec. III.B.

A. Formulations of the Proposed VF-LCB

1. *Single-Fidelity Lower Confidence Bounding Function*

LCB is one of the most famous infill sampling criteria [32], in which the objective is to locate the new sampling point based on a line combination of the predicted value and the standard error. The LCB expression is presented as,

$$\text{lcb}(\boldsymbol{x}) = \hat{y}(\boldsymbol{x}) - b\hat{\sigma}(\boldsymbol{x}) \tag{12}$$

where $\hat{y}(\boldsymbol{x})$ and $\hat{s}(\boldsymbol{x})$ are the estimated objective function value and the corresponding standard error at the point $\boldsymbol{x}$, b is a user-defined parameter that balances the exploration and exploitation, and the values for $b = 2$ and $b = 2.5$ are reported by Cox and John [32]. With the LCB function minimizing, locations of the new sample points that have either high prediction uncertainty or low function values are favored by Eq. (12). A larger value of b means more emphasis on the high prediction uncertainty, thereby forcing a more global searching strategy. On the contrary, the algorithm turns more attention to the local regions with a smaller b value.

2. *Variable-Fidelity Lower Confidence Bounding Function*

A VF-LCB function, which is an extension of the single-fidelity LCB function to determinate both location and fidelity level of the subsequent evaluation, is formulated. The uncertainty of the VF metamodel is quantified by considering the uncertainties from both LF metamodel and scaling functions. Similar to the single-fidelity LCB function, the VF-LCB function is also derived as a linear combination of the predicted values and errors. Moreover, the CoV statistical information is introduced to calculate the weights, aiming to objectively balance the global and local search. The VF-LCB function can be expressed as,

$$\text{LCB}_{\text{vf}}(\boldsymbol{x}, t) = \omega_f \hat{y}_{\text{vf}}(\boldsymbol{x}) - \omega_{\text{rmse}} \hat{\sigma}(\boldsymbol{x}, t) CR(t) \tag{13}$$

where t represents the fidelity level. $\hat{y}_{\text{vf}}(\boldsymbol{x})$ is the predicted value from the VF metamodel, which is calculated by Eq. (10). $\hat{\sigma}(\boldsymbol{x}, t)$ is the uncertainty of the t-level metamodel at point $\boldsymbol{x}$, which can be calculated by,

$$\hat{\sigma}(\boldsymbol{x}, t) = \begin{cases} \hat{\sigma}_l(\boldsymbol{x}), & t = 1 \\ \sqrt{\hat{\sigma}_l^2(\boldsymbol{x}) + \hat{\sigma}_C^2(\boldsymbol{x})}, & t = 2 \end{cases} \tag{14}$$

In Eq. (13), the first term is the product of the predicted value of the VF metamodel and a coefficient, which is only a function of design variables, whereas the second term is the function of design variables $\boldsymbol{x}$ and fidelity level t. Therefore, the VF-LCB values of different fidelity levels depend only on the uncertainties of the VF metamodel, which are expressed in Eq. (14). In Eq. (14), the uncertainty of the VF metamodel is the function of the uncertainties of the LF metamodel and the scaling function. If the uncertainty of the LF metamodel is large enough to achieve the minimum VF-LCB value, it means that adding an LF sample will improve the VF metamodel accuracy most; otherwise, an expensively computational HF sample will be added. The weighting parameters ω_f and ω_{rmse} represent the emphasis for searching on the global and local region, respectively. As a result, minimizing the VF-LCB will adaptively determine the fidelity levels and objectively balance the global and local searching. Some vital parameters are elaborated below.

1) *The weighting parameters ω_f and ω_{rmse}*: In the single-fidelity LCB function, the weighting parameter, which is represented as b in

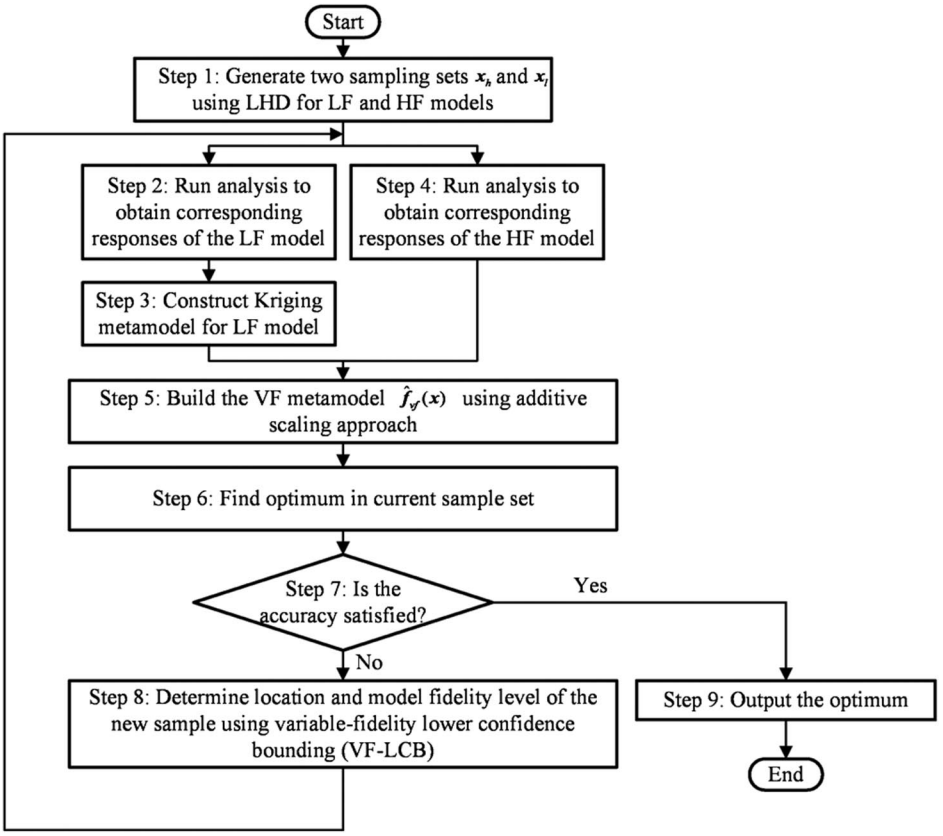

Fig. 1 Flowchart of the proposed VF-LCB approach.

the formulation, is usually subjectively determined by experience or experiment [37]. Here a novel weighting scheme is developed for a more objective searching process, where CoV is introduced to describe the distribution of local optimum and global accuracy of the established VF metamodels. The calculation process is as follows: Then the CoV of the prediction value and prediction uncertainty are defined as,

$$\text{CoV\_}f = \frac{\sigma_f}{\mu_f}, \qquad \text{CoV\_rmse} = \frac{\sigma_{\text{rmse}}}{\mu_{\text{rmse}}} \tag{15}$$

where CoV_f and CoV_rmse represent the CoV of the predictive values and the root mean square errors (RMSE) of the VF metamodel, respectively. σ_f and σ_{rmse} are the standard deviation of the predictive values and the RMSE, respectively. μ_f and μ_{rmse} are the average of the predictive values and the RMSE. Compared with expensive simulations, the cost of obtaining the predicted value and RMSE can be negligible because the predicted values and the RMSE are directly predicted from the VF metamodel.

Obviously, when the CoV of predictions is larger, the algorithm should pay more attention to the local exploitation. While the CoV of uncertainty is larger, the algorithm should focus more on global exploration. Therefore, the weights of prediction and uncertainty can be defined as,

$$\omega_f = \frac{\text{CoV\_}f}{\text{CoV\_}f + \text{CoV\_rmse}}, \qquad \omega_{\text{rmse}} = \frac{\text{CoV\_rmse}}{\text{CoV\_}f + \text{CoV\_rmse}} \tag{16}$$

where ω_f and ω_{rmse} are the prediction and uncertainty weighting factors of the current VF metamodel.

Because the HF model is more accurate than the LF one, the CoV of HF model is more reasonable to indicate the distribution of the actual function in the global and local regions. CoV is a statistic that measures the degree of variation of observations in each item, which is used to measure the variation of the current metamodel's prediction and uncertainty. The CoV of prediction reflects the number of local optimal values of the function, and the CoV of uncertainty reflects the accuracy of the function. When the dispersion of function values is large, that is, the function value changes drastically, it is better to focus on the accuracy around the target minimum value. On the contrary, when the dispersion of standard deviations is large, it is more desirable to conduct explorations globally to eliminate errors of the metamodel. Therefore, the weighting parameter, which is determined by the characteristics (prediction value and prediction uncertainty) of the established VF metamodel, can balance the exploitation and exploration objectively.

2) *Ratio of cost* $CR(t)$: $CR(t)$ represents the computational cost ratio of a response evaluation between the model of fidelity level t and the highest fidelity level model.

$$CR(t) = \frac{C_h}{C(t)} \tag{17}$$

where C_h and $C(t)$ are the computational cost of a response evaluation for the HF model and tth-level fidelity model, respectively. For the VF metamodel with two fidelity levels, the cost ratio can be expressed as,

$$CR(t) = \begin{cases} c & t = 1 \\ 1 & t = 2 \end{cases} \tag{18}$$

where $c \geq 1$, which means that the computational cost of an LF sample point is lower than that of a HF one. The inclusion of $CR(t)$ in Eq. (12) is to consider the influence of computational cost for a different fidelity model, and select the new input sample of the computationally cheap model with high uncertainty; that is, if there is a point that has identical uncertainty between the LF model and HF model, the algorithm will select the model with less computational cost.

3. Constraint Problem Handling

For the problem with computationally expensive constraints, the constraints are also constructed by the VF metamodel, which is a function of the design variables and fidelity levels. The prediction for the constraints at a point can be considered as a normal distribution,

$$G(\boldsymbol{x}, t) \sim N[\hat{g}(\boldsymbol{x}), s_g^2(\boldsymbol{x}, t)] \tag{19}$$

where $s_g^2(\boldsymbol{x}, t)$ is the uncertainty of the constraint metamodel due to the lack of tth-level fidelity samples. Therefore, the probability of satisfying the constraint can be expressed as,

$$P[G(\boldsymbol{x}, t) \le 0] = \Phi\left(\frac{0 - \hat{g}(\boldsymbol{x})}{s_g^2(\boldsymbol{x}, t)}\right) \tag{20}$$

Considering the probability to the VF-LCB function, its constraint formulation can be expressed as,

$$\mathrm{CLCB}_{\mathrm{vf}}(\boldsymbol{x}, t) = \begin{cases} \mathrm{LCB}_{\mathrm{vf}}(\boldsymbol{x}, t) \prod_{i=1}^{N_C} \frac{1}{P[G(\boldsymbol{x},t) \le 0]}, & \text{if } \mathrm{LCB}_{\mathrm{vf}}(\boldsymbol{x}, t) > 0 \\ \mathrm{LCB}_{\mathrm{vf}}(\boldsymbol{x}, t) \prod_{i=1}^{N_C} P[G(\boldsymbol{x}, t) \le 0], & \text{if } \mathrm{LCB}_{\mathrm{vf}}(\boldsymbol{x}, t) \le 0 \end{cases} \tag{21}$$

where N_C represents the number of constraints. Through minimizing Eq. (21) the location of the new sample that has more probability of satisfying the constraints is favored.

B. Detailed Steps of the Proposed VF-LCB Approach

The specific details of each step of the VF-LCB approach are described below.

Step 1: Because the LF model can indicate the trends of the system at a considerable reduced computational cost, an initial sampling set $\boldsymbol{x}_l = \{\boldsymbol{x}_1^l, \boldsymbol{x}_2^l, \ldots, \boldsymbol{x}_{m_l}^l\}$ with relatively large sample points is generated to guarantee the accuracy of the LF model. For the HF model, a set $\boldsymbol{x}_h = \{\boldsymbol{x}_1^h, \boldsymbol{x}_2^h, \ldots, \boldsymbol{x}_{m_h}^h\}$ with the significantly smaller number of sample points is generated to establish the scaling function. In this paper, the Latin hypercube design (LHD) method is employed to generate the sample sets for both HF and LF models.

Step 2: Based on the sample sets of the LF model generated in step 1, numerical simulations are carried out to get the actual LF responses $\boldsymbol{f}_l = \{f_1^l, f_2^l, \ldots, f_{m_l}^l\}$.

Step 3: According to the obtained sample data, an LF kriging metamodel is constructed using DACE toolbox.

Step 4: Based on the sample sets of HF model generated in step 1, the actual HF responses $\boldsymbol{f}_h = \{f_1^h, f_2^h, \ldots, f_{m_h}^h\}$ are obtained by running the HF analyses.

Step 5: After obtaining the sample data, the VF metamodel is built using the additive scaling approach described in Sec. II.B.

Step 6: In this step, an optimum is obtained in the current sample set.

Step 7: After obtaining the current global optimum, a terminal criterion is tested. If satisfied, the algorithm goes to step 2; otherwise, it goes to step 9. The terminal criterion used in the numerical examples is expressed as,

$$|y_n - y| \le \varepsilon \tag{22}$$

where y_n represents the global optimum obtained in the current iteration, y is the actual global optimum that is known in advance, and ε is the absolute error between the predicted optimum and the actual optimum that is defined by the engineer. For the practical engineering problems with unknown optimum, the following termination criterion is employed,

$$\begin{cases} |y_n - y_{n-1}| \le \gamma, |y_{n-1} - y_{n-2}| \le \gamma \\ W = W_{\max} \end{cases} \tag{23}$$

where y_{n-2}, y_{n-1}, and y_n are the optimal solutions of VF metamodels obtained in the $(n-2)$th, $(n-1)$th, and nth iteration; γ is the relaxation factor; W is the number of iteration; and $W_{\max}$ is the maximum number of iteration, which is determined according to the limitation of computational cost.

If the terminal criterion is not satisfied, the algorithm goes to step 8 and starts a new iteration; otherwise, it goes to step 9 and outputs the optimum.

Step 8: Calculate the minimum of VF-LCB function using the genetic algorithm (GA) [50]. The settings of GA in this work are as follows, the maximum generation is set to be 100, and the population is 40. The probability of mutation and crossover are 0.01 and 0.95, respectively. Because differential optimizers usually have different pros and cons, some other optimizers, like particle swarm optimization (PSO), can also be employed instead of GA. After the calculation, the fidelity level is selected according to the minimum of the VF-LCB function values. Then the location of the sample point, which has the minimum of the VF-LCB function, is added to the sampling set. When faced with the constraint problems, the constraint formulation is employed instead.

Step 9: Once the termination criterion is satisfied, the algorithm provides the final optimum.

IV. Examples and Results

In this section, eight numerical examples and one engineering case are adopted to illustrate the applicability and efficiency of the proposed VF-LCB approach. These examples are also solved using the other five existing methods for comparison: 1) single-fidelity EI [31], 2) single-fidelity LCB [32], 3) augmented expected improvement (AEI) [40], 4) variable-fidelity EI (VF-EI) [42], and 5) multifidelity optimization (MFO) [51]. Among them, EI and LCB are famous single-fidelity surrogate-based optimization methods, which are used to test the efficiency of the variable-fidelity model. AEI, VF-EI, and MFO are comparable variable-fidelity approaches,

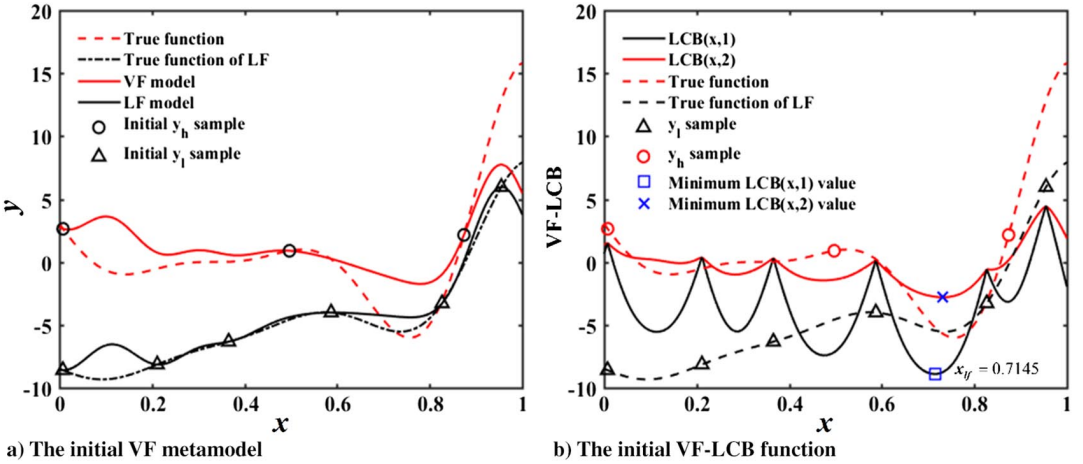

a) The initial VF metamodel b) The initial VF-LCB function

Fig. 2 Initial VF metamodel and the corresponding VF-LCB function.

Table 1 The updating process of the proposed VF-LCB approach for the illustrative test case

Updating cycle	ω_f, ω_{rmse}	Added sample	Fidelity level	Best-observed hi-fi function value
1	0.5797, 0.4203	0.7145	1 (LF)	−2.4956
2	0.6158, 0.3842	0.7385	2 (HF)	−5.9076
3	0.4442, 0.5558	0.7007	2 (HF)	−5.9558
4	0.4452, 0.5548	0.2718	2 (HF)	−5.9557
5	0.4655, 0.5345	0.7548	1 (LF)	−5.9661
6	0.4513, 0.5487	0.7586	2 (HF)	−6.0209
7	0.4131, 0.5869	0.7582	1 (LF)	−6.0209
8	0.4035, 0.5965	0.7570	2 (HF)	−6.0207

in which VF-EI is the state-of-the-art multiple-fidelity approach that employs the EGO algorithm to execute the optimization process.

A. Illustrative Case

A one-dimensional numerical case [52] is applied to illustrate the detailed process of the proposed approach in this subsection. The numerical case is given as,

$$\begin{aligned} \min\ y_h &= (6x-2)^2 \sin(12x-4), \quad x \in [0,1] \\ y_l &= 0.5y + 10(x-0.5) - 5 \end{aligned} \tag{24}$$

where y_h denotes the HF analytical function, and y_l denotes the LF analytical function. The analytical global optimum is $y = -6.0207$ at the point $x^* = 0.7573$. As a demonstration, the computational cost

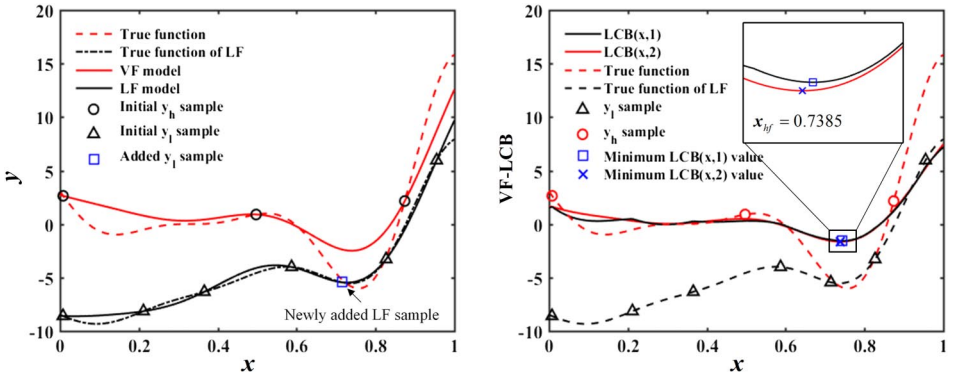

a) The VF metamodel refined by adding a LF sample point (left) and the corresponding VF-LCB functions (right)

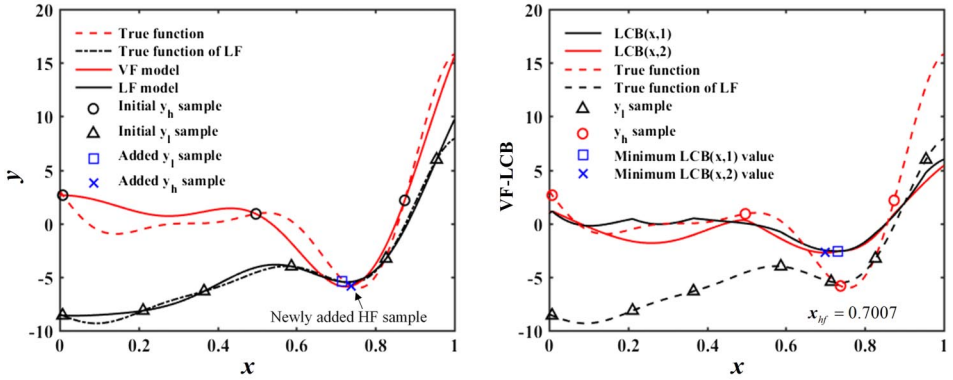

b) The VF metamodel refined by adding a LF sample and a HF sample (left) and the corresponding VF-LCB functions (right)

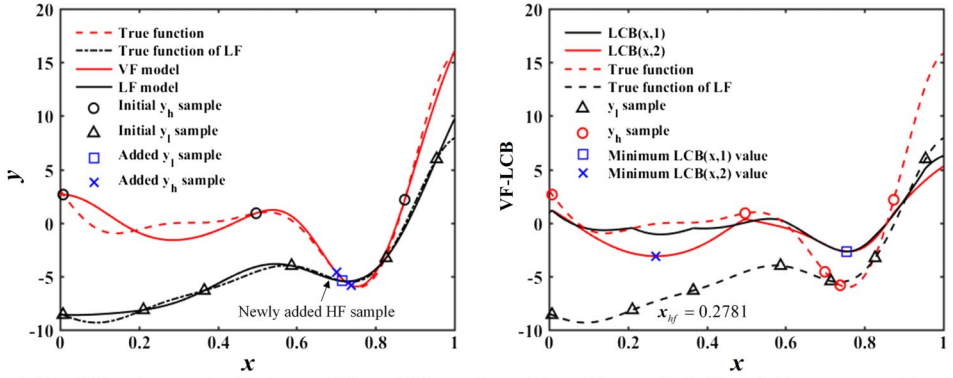

c) The VF metamodel refined by adding a LF sample and two HF sample (left) and the corresponding VF-LCB functions (right)

Fig. 3 Refinement process of optimization of illustrative study based on the proposed VF-LCB in the second, third, and fourth iteration.

ratio between HF and LF models is assumed to be 4. The impact of different cost ratios will be discussed in Sec. IV.B.

In the first stage, two initial sample sets contained with three HF sample points and six LF sample points are generated as $\boldsymbol{S}_{\text{hf}} = \{0.0079, 0.4971, 0.8741\}$, $\boldsymbol{S}_{\text{lf}} = \{0.0075, 0.2115, 0.3658, 0.5872, 0.8268, 0.9548\}$. Based on the initial sample points, an initial VF metamodel is built, as shown in Fig. 2a. Although the LF model is not accurate enough, it has a similar trend compared with the HF model. Once the initial VF metamodel is constructed, the proposed approach begins the iterative optimization process. The changes of the weighting parameters are summarized in Table 1. As observed from Table 1, in the first iteration the weighting parameters are $\{0.5797, 0.4203\}$, which means that in the first process the approach focuses the local search for the global optimum. Figure 2b shows the distribution of the VF-LCB function in the design space. As can be seen from Fig. 2b, the uncertainties of the LF and VF metamodels are relatively large at the untried points. But with the effect of the cost ratio, the LCB function of the LF model, that is, LCB$(\boldsymbol{x}, 1)$, is lower than the LCB$(\boldsymbol{x}, 2)$. The minimum of the LF model is lower than that of the HF model, which implies that adding LF sample can make more improvement to the VF metamodel than adding HF sample in this iteration, and so a new LF sample point at $x = 0.7145$ should be added to the LF sample set and then rebuild the VF metamodel. The new VF metamodel refined by adding an LF sample point is represented in Fig. 3a (left), and the weighting parameters are $\{0.6158, 0.3842\}$. The LF kriging function is getting accurate in the optimal region, and the corresponding trend in the HF model is slightly revised. In the second iteration, as the minimum of VF-LCB function in HF is smaller, as shown in Fig. 3a (right), a HF sample point at $x = 0.7385$ is added to the HF sample set. After adding a HF sample and an LF sample the VF metamodel becomes more accurate, as shown in Fig. 3b (left). The weighting parameters change to $\{0.4442, 0.5558\}$ in the third iteration, which means that the proposed approach changes the emphasis from local to global. According to the guidance of the VF-LCB function in the third iteration, another HF sample point in the optimal region at $x = 0.7007$ should be added. The VF metamodel has featured the similar trend in the optimal region after adding two HF sample points and one LF sample point, as shown in Fig. 3c (left). In this time, the uncertainty of HF model at the point $x = 0.2781$ is large enough that the VF-LCB value at this point reaches the minimum, and so a new HF sample point at $x = 0.2781$ should be added to the HF sample set.

The remaining refinement process of the VF metamodel is sketched in Fig. 4. The VF metamodel is getting more accurate by adding a HF sample point in the sixth iteration and an LF sample point in the seventh iteration. Finally, after adding three LF samples and five HF samples in total, the updating process terminates, and a global

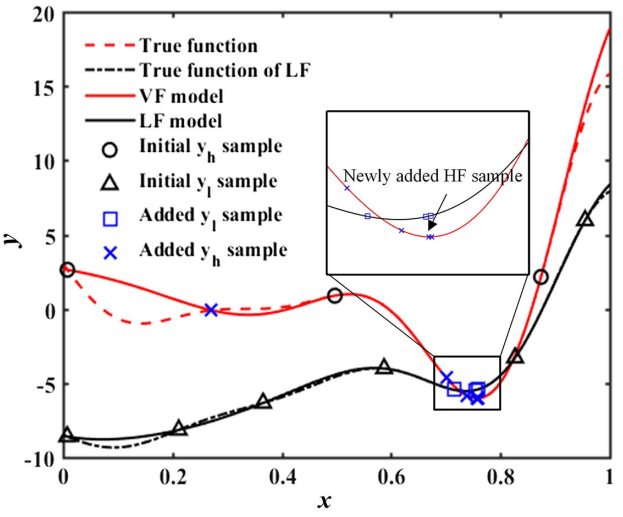

Fig. 5 The refinement of the VF metamodel in the last iteration.

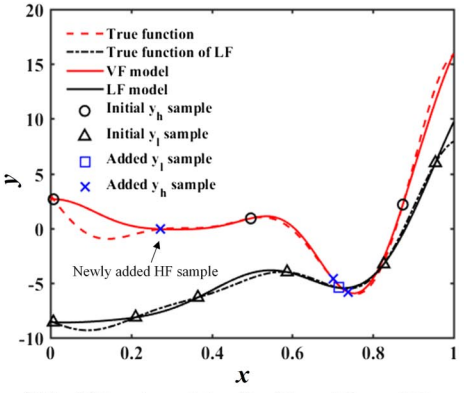

a) The VF metamodel refined by adding a LF sample and three HF sample

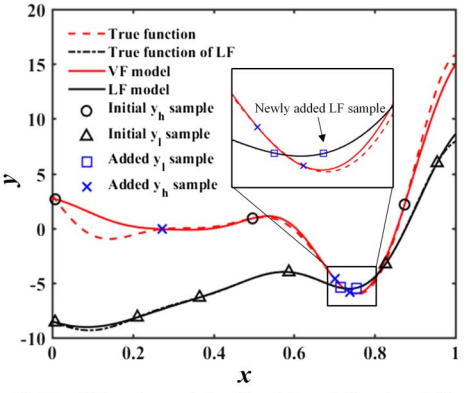

b) The VF metamodel refined by adding two LF sample and three HF sample

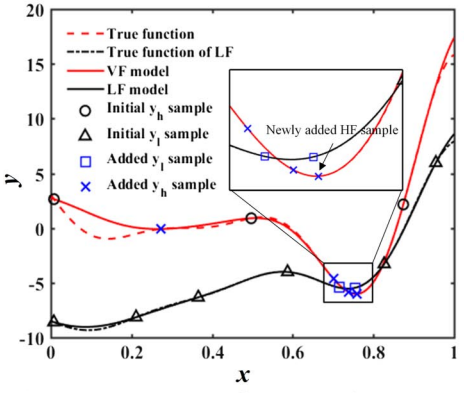

c) The VF metamodel refined by adding two LF sample and four HF sample

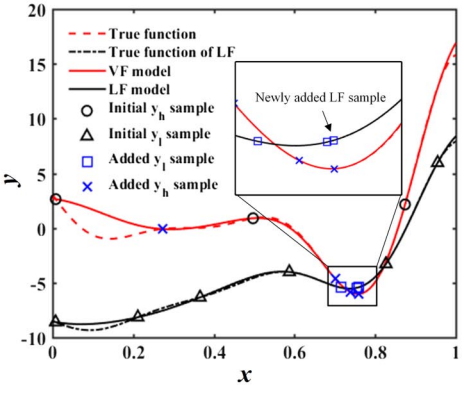

d) The VF metamodel refined by adding three LF sample and four HF sample

Fig. 4 The refinement of the VF metamodel in the fourth, fifth, sixth, and seventh iteration.

Table 2 Compared results for VF optimization using EI, AEI, VF-EI, and VF-LCB approaches

Test case	Test approach	Average No. of total sample points		TC	STD of cost	Difference with optima, %
		Low-fi sample	Hi-fi sample			
Case 1	EI	/	11.8	11.80{4}	1.619{4}	0.00012
	LCB	/	10.4	10.40{2}	0.699{2}	0.00019
	AEI	10.2	12	14.55{6}	9.208{6}	0.00092
	VF-EI	9.7	8.4	10.83{3}	2.148{5}	0.00083
	MFO	8.6	10.3	12.45{5}	**0.665**{1}	0.0439
	VF-LCB	6.2	**7.5**	**9.050**{1}	1.457{3}	0.00011
Case 2	EI	/	11.8	11.80{6}	1.619{4}	0.00012
	LCB	/	10.4	10.40{4}	0.699{2}	0.00019
	AEI	8.6	7.6	9.750{3}	2.386{6}	0.00045
	VF-EI	10.2	7.9	10.45{5}	1.833{5}	0.00029
	MFO	9.1	6.8	9.075{2}	1.131{3}	0.0495
	VF-LCB	9.9	**5.4**	**7.880**{1}	**0.680**{1}	0.00017
Case 3	EI	/	11.8	11.80{3}	1.619{5}	0.00012
	LCB	/	10.4	**10.40**{1}	**0.699**{1}	0.00019
	AEI	37.2	15.4	24.70{6}	9.495{6}	0.00030
	VF-EI	10.4	9.6	12.20{4}	1.549{4}	0.00024
	MFO	9.8	**9.3**	11.75{2}	1.424{3}	0.0202
	VF-LCB	12.3	11.8	14.88{5}	1.226{2}	0.00010
Case 4	EI	/	29.5	29.50{3}	5.318{4}	0.021
	LCB	/	34.5	34.50{5}	**3.749**{1}	0.012
	AEI	62.6	29.7	45.35{6}	11.06{6}	0.026
	VF-EI	20.5	23.2	28.33{2}	4.031{3}	0.022
	MFO	27.2	23.5	30.30{4}	5.677{5}	0.029
	VF-LCB	21.2	**21.3**	**26.60**{1}	3.781{2}	0.022
Case 5	EI	/	64.6	64.60{3}	30.48{3}	0.058
	LCB	/	65.9	65.90{4}	**6.871**{1}	0.064
	AEI	51.6	40.0	52.90{2}	74.43{6}	0.043
	VF-EI	143.7	35.2	71.13{5}	34.79{4}	0.055
	MFO	64.2	61.1	77.15{6}	40.96{5}	0.050
	VF-LCB	123.7	**19.5**	**50.43**{1}	20.06{2}	0.057
Case 6	EI	/	72.6	72.60{5}	93.09{6}	2.227
	LCB	/	68.7	68.70{4}	58.84{4}	1.85
	AEI	99	65.8	90.55{6}	64.07{5}	2.480
	VF-EI	54	35.8	49.30{2}	15.20{3}	2.094
	MFO	42.5	41.1	51.73{3}	**9.819**{1}	2.037
	VF-LCB	72.4	**22.7**	**40.80**{1}	11.67{2}	1.559
Case 7	EI	/	24	24.00{5}	16.68{5}	0.023
	LCB	/	20.5	20.50{2}	3.340{2}	0.007
	AEI	29.9	15	22.48{3}	**2.926**{1}	0.014
	VF-EI	33.9	15.1	23.58{4}	6.534{4}	0.020
	MFO	18.5	32.4	34.25{6}	33.94{6}	1.564
	VF-LCB	24.1	**13.3**	**19.33**{1}	4.522{3}	0.017
Case 8	EI	/	87.1	87.10{5}	70.22{6}	0.235
	LCB	/	87.9	87.90{6}	54.72{5}	0.308
	AEI	41.2	41.2	51.50{4}	29.49{4}	0.215
	VF-EI	47.2	36.9	48.70{3}	14.54{3}	0.253
	MFO	50	25.6	38.10{2}	**3.143**{1}	0.974
	VF-LCB	33.9	**17.1**	**25.58**{1}	3.338{2}	0.193

Table 3 Average ranking results for the four comparative approaches

Metric	EI	LCB	AEI	VF-EI	MFO	VF-LCB
TC	4. 25	3.5	4.5	3.5	3.75	**1.5**
STD of TC	4.625	2.25	5	3.875	3.125	**2.125**

optimum with a predefined difference has been found. Refinement of the last iteration is shown in Fig. 5; it can be seen that it is accurate enough in the global optimal region although in other regions there are differences between VF metamodel and the analytical function.

As can be seen from the weighting item in Table 1, in the early stage, the approach pays more attention to the local searching and then it turns to focus on the global uncertainty with new points added. It is shown that the proposed approach can adaptively adjust the weight between global exploration and local exploitation based on the VF metamodel. According to the results, the proposed approach not only can combine the information of the LF model and the HF model to adaptively determine the location and fidelity of the newly selected sample points, but also can adaptively adjust the weights of global and local search to improve the efficiency.

B. Additional Numerical Examples

In this subsection, eight commonly used numerical examples, that is, six unconstrained cases and two constrained cases from [20,52–55], are employed to illustrate the effectiveness and efficiency of the proposed VF-LCB approach. The expressions of each test function are described in Appendix A. The computational cost ratio between a HF evaluation and an LF one for all the test cases is set to be 4. The influences of different cost ratios are discussed at the end of this subsection.

In all of these cases, the numbers of the initial HF and LF sample points are set to be $3d$ and $6d$, respectively, where d represents the dimension of the design variable. Considering the randomness of the LHD method and GA, all problems solved by using EI, LCB, AEI, VF-EI, MFO, and VF-LCB approaches are repeated 10 times.

The efficiency of these approaches is measured by the total analytical function calls. Then the total cost is defined by,

$$\mathrm{TC} = \frac{1}{CR(2)}\mathrm{HFC} + \frac{1}{CR(1)}\mathrm{LFC} \tag{25}$$

where HFC and LFC represent the numbers of function calls for HF and LF models, respectively. $CR(2)$ and $CR(1)$ are cost ratios of HF evaluation and LF evaluation calculated by Eq. (17). The standard deviation (STD) of the total cost is used to gauge the robustness of each approach. The accuracy of each approach is represented by the relative difference between the obtained optimized solution and analytical optimum. All the computations of six approaches are

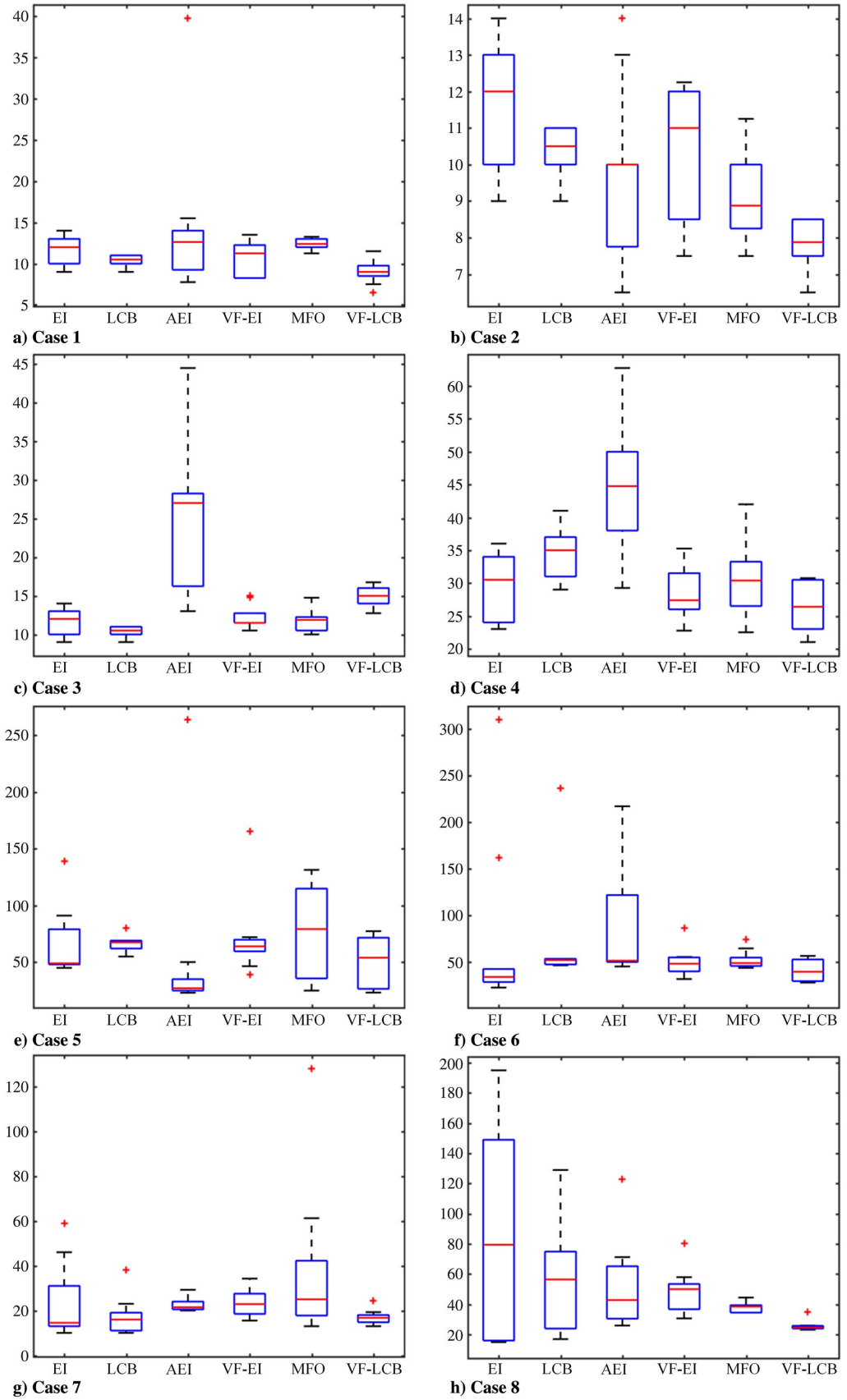

Fig. 6 Comparison results of different cases for the proposed VF-LCB approach and other approaches.

Table 4 Comparison results for the four approaches in consideration of different cost ratios

Case	Approach	$CR = 2$	$CR = 4$	$CR = 10$	$CR = 100$
Case 1	EI	11.8	11.80	11.80	11.800
	LCB	**10.4**	10.40	10.40	10.400
	AEI	13.2	14.55	9.76	9.764
	VF-EI	12.8	10.83	8.56	8.211
	MFO	14.6	11.63	9.76	8.893
	VF-LCB	11.7	**9.05**	**7.69**	**7.137**
Case 4	EI	29.5	29.50	29.50	29.500
	LCB	34.5	34.50	34.50	34.500
	AEI	35.9	45.35	25.15	24.712
	VF-EI	**29.3**	28.33	**23.29**	23.924
	MFO	30.9	30.30	26.49	22.212
	VF-LCB	31.7	**26.60**	24.24	**20.946**

Table 5 Adjusted p-values obtained in the numerical examples by Bergmann-Hommel's dynamic procedure

i	Hypothesis	p_i
1	EI vs VF-LCB	**0.0162**
2	LCB vs VF-LCB	0.0614
3	AEI vs VF-LCB	**0.0033**
4	VF-EI vs VF-LCB	**0.0075**
5	MFO vs VF-LCB	**0.0325**

conducted in the MATLAB environment on the computational platform with a 3.70 GHz Intel (R) Core (TM) i7 CPU and 16 GB RAM.

Table 2 summarizes the results; the best results in each test case are marked in bold and the comparable ranks in each test case are given in braces. It is observed from Table 2 that the relative errors all achieved the defined values, which implies that all the compared approaches reach the identical accuracy. In terms of the number of HF sample points, it is shown that the proposed VF-LCB approach can reduce the optimization cost in seven cases compared with the single-fidelity EI and LCB approach, and in cases 2, 5, 6, and 8 the proposed approach reduces more than 50% of HF computational cost compared with the single-fidelity approaches. As for the total cost, the proposed approach can improve the computational efficiency in all the cases except for the case 3, which has a poor correlation between LF function and HF function. The proposed approach shows great efficiency especially in cases 2, 6, and 8 compared with the standard EI method. Compared with the VF-EI approach, the proposed approach reduces more than 20% of the total computational cost for cases 2, 5, and 8. Compared with the AEI approach, the proposed approach reduces more than 40% of the total cost for cases 1, 3, 4, 6, and 8. For the robustness of these approaches, the proposed VF-LCB approach shows desirable robustness among all eight cases. The single-fidelity LCB performs the best on robustness in cases 3, 4, and 5; however, the MFO approach has the best robustness in cases 1, 6, and 8. But it performs worse in test cases 4, 5, and 7. The robustness of the AEI approach is worse for most of the test cases.

Table 3 summarizes the average ranking results of the six comparative approaches in the metrics of efficiency and robustness. The average ranks of the proposed VF-LCB approach are the best for both the efficiency metric and robustness metric. The VF-EI approach and the single-fidelity LCB approach rank the second for efficiency. AEI performs the worst in the efficiency metric. Regarding the robustness, the single-fidelity LCB approach and MFO show desirable performance, and the AEI performs the worst among six approaches. In conclusion, the proposed VF-LCB approach reduces the computational cost but maintains a desirable robustness.

Figure 6 depicts the boxplots of the total computational cost for the proposed VF-LCB approach and the other five existing approaches under the eight different cases, where lower (25%) and upper (75%) quartile values are also shown. The dotted lines extending from the top and bottom of the box represent 1.5 times of the interquartile range. Data that lie out of this range are considered as outliers and are marked by the symbol "+." From Fig. 6 it can be observed that the median of VF-LCB approach is lower than all other approaches in cases 1, 2, 4, and 8. In most of the cases, the interquartile ranges of the proposed approach are less than the other approaches, which illustrates the robustness of the proposed approach. The number of extreme values of the proposed approach is less than that of the other methods, especially in cases 5 and 6, which also validates the robustness of the VF-LCB approach.

To study the influence of different cost ratios, $CR = 2$, $CR = 4$, $CR = 10$, and $CR = 100$ are adopted to test the efficiency of the proposed approach for cases 1 and 4. The results of the total computational cost are listed in Table 4, and the best results are marked in bold. From Table 4, it can be compared in test case 1 that the total computational cost of the proposed approach is always the least, which demonstrates the efficiency and applicability of the proposed approach. For the results of case 4, the VF-EI outperforms the other approaches when $CR = 2$ and $CR = 10$, whereas the VF-LCB approach has the best efficiency for $CR = 4$ and $CR = 100$. With the cost ratio increasing, each VF optimization approach obtains the global optimum with less computational total cost.

To test whether the difference between the proposed approach and the other test approaches over the total cost is statistically significant or not, the procedure developed by Garcia and Herrera [56] is employed and a Friedman test [57] is performed, in which the Bergmann-Hommel procedure [58] is adopted to calculate adjusted p-values. The results are summarized in Table 5. The null hypothesis is that there is no difference among the proposed approach and the other approaches. All the adjusted p-values are less than 0.05 except for the single-fidelity LCB approach, indicating that there are differences between the proposed VF-LCB approach and the other three VF-based approaches in efficiency.

C. Design of Micro-Aerial Vehicle Fuselage

In this section, the design of MAV fuselage [12,59] is employed to illustrate the efficiency of the proposed approach. The structure of MAV is shown in Fig. 7. It is usually used for military reconnaissance to transmit real-time images and perform various important tasks due to its small size, wide cruising range and long flight time. The fuselage of MAV is the main bearing structure. To meet the demand of carrying capability and good endurance, MAV fuselage should be made of lightweight and durable materials. This engineering design problem focuses on the structural design optimization of MAV fuselage.

In this example, the fuselage is made by lightweight ABS materials. The simplified geometry model of MAV fuselage with general dimension labels is shown in Fig. 8. The Young's modulus of the ABS materials is 1900 $\mathrm{N/mm^2}$ and Poisson's ratio is 0.3.

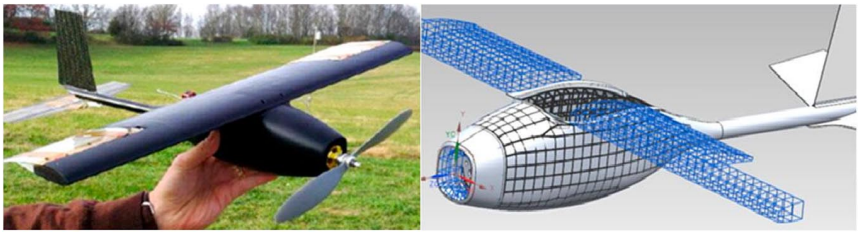

Fig. 7 Micro-aerial vehicle.

In this paper, ANSYS 18.0 is employed as a simulation tool for evaluating the corresponding responses. As shown in Fig. 9, the fuselage is mainly affected by three loadings: the weight of the engine in the front ($F_{\text{Motor}} = 5.9$ N), the payload, and the weight of the tail ($F_{\text{Tail}} = 2.7$ N). The payload is represented as a distributed loading $F_{\text{Payload}} = 0.1$ N/mm^2 on the internal surface of the fuselage. The loadings of F_{Motor} and F_{Tail} are simplified as concentrated loads acting at their centers of gravity, which are applied in ANSYS with weightless rigid link elements. The weight of the wings is too small to be negligible. A small area at the bottom of the fuselage is fixed to model the contact area when landing or crashing.

In the optimization process, the objective is to minimize the maximum deformation along the z-axis. There are two constraints to guarantee a proper design: the maximum equivalent stress and a total volume restrict. The optimization problem is expressed as follows:

$$\begin{aligned}
&\min\ f = u_z(A_1, A_2, A_3, D, L, t)\\
&\text{s.t. } g_1 = V \le 200\ \text{cm}^3 \quad g_2 = \sigma \le 36\ \text{MPa}\\
&\text{where } 46\ \text{mm} \le A_1 \le 50\ \text{mm}; \qquad 85\ \text{mm} \le A_2 \le 95\ \text{mm}\\
&46\ \text{mm} \le A_3 \le 50\ \text{mm}; \qquad 40\ \text{mm} \le D \le 50\ \text{mm}\\
&250\ \text{mm} \le L \le 260\ \text{mm}; \qquad 6\ \text{mm} \le t \le 8\ \text{mm}
\end{aligned} \tag{26}$$

A simulation model with about 8500 nodes is selected as the LF model, whereas the HF simulation model has about 73,000 nodes, as shown in Fig. 10. The computational time of the HF simulation model is about six times that of an LF simulation model. Therefore, the cost ratio is set to 6.

The proposed approach and other five approaches are all applied to solve this engineering problem. The optimization begins with 18 HF initial sample points and 36 LF initial sample points. Table 6 gives optimal results of the design variables for each solving approaches. The corresponding objective values, constraint values, and the numbers of simulation calls are summarized in Table 7, where LFC and HFC represent numbers of LF and HF simulation calls. TC is the total cost calculated by Eq. (25).

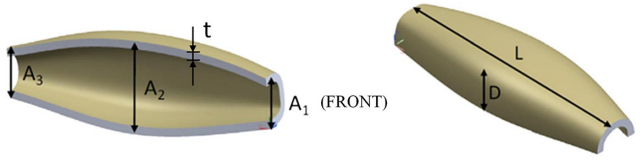

Fig. 8 The geometry model of MAV fuselage with general dimension labels.

Table 6 The optimal design points of different approaches

Approach	A_1	A_2	A_3	D	L	t
EI	49.3933	85.0352	40.1837	40.0001	250.0110	7.2589
LCB	46.0193	85.0067	40.0038	40.0000	250.0012	7.3740
AEI	46.4380	85.0069	40.8797	40.0037	250.0007	7.3039
VF-EI	46.0273	85.1638	43.2263	40.0054	250.5016	7.2803
MFO	47.0689	86.4283	42.0138	40.0362	250.0039	7.1822
VF-LCB	47.4311	85.0004	40.080	40.0079	250.0017	7.3456

Table 7 The corresponding objective values, constraint values, and the numbers of simulation calls for different approaches

Approach	u_z	g_1	g_2	LFC	HFC	TC
EI	4.2046	198.8793	30.1894	/	53	53
LCB	4.0410	199.9653	29.4766	/	200	200
AEI	4.1310	198.8729	31.1810	63	63	73.5
VF-EI	4.1530	199.8812	32.3557	110	60	78.33
MFO	4.2857	199.2668	31.8889	37	42	48.17
VF-LCB	4.0918	199.9339	30.9524	53	24	32.83

From Table 7, it can be observed that all the six approaches satisfy the termination criterion and obtain the optimized design solution with feasible constraints. The single-fidelity LCB approach obtains the best optimized solution among the six methods, but it takes 200 TC to get that best result. The proposed VF-LCB method gets the second best objective value with only about 32 TC, which reduces nearly 80% compared with the single-fidelity LCB. Compared with the VF-EI and AEI methods, the proposed approach gets a better result with fewer computational TC. In terms of HFC, the proposed approach uses the least simulation calls, and it is improved by about 90% compared with the single-fidelity LCB method, and 36% compared with the VF-EI, which proves the efficiency of the proposed approach. For the number of TC, the proposed approach has reduced by about 55% compared with the multiple-fidelity AEI

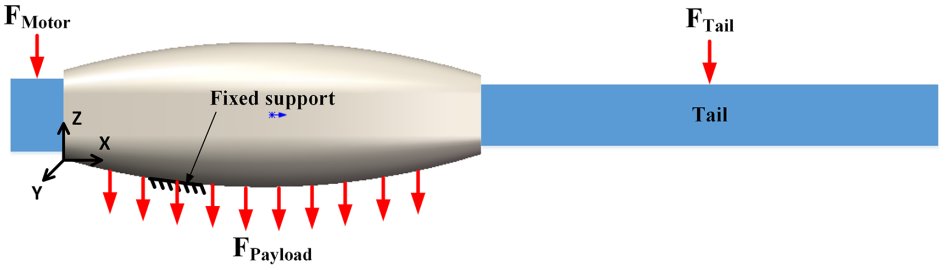

Fig. 9 Loading and boundary conditions of the MAV fuselage.

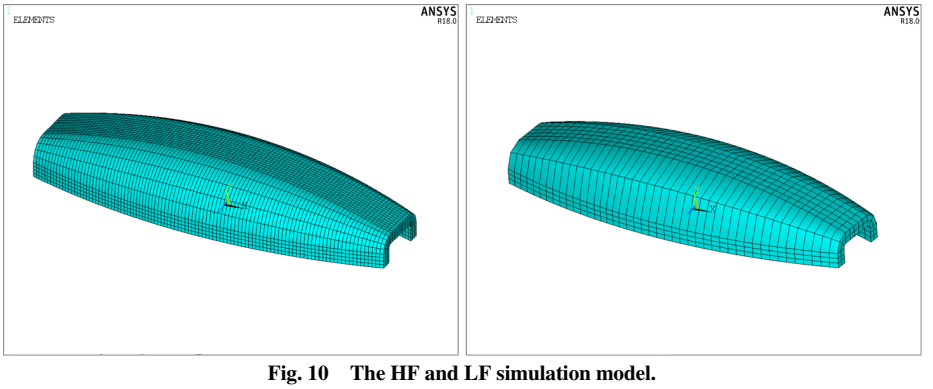

Fig. 10 The HF and LF simulation model.

approach, and about 58% less than the VF-EI method. Compared with the other methods, the MFO gets a worse-optimized solution when converges. In conclusion, the proposed approach shows great potential in reducing the computational cost and, at the same time, obtaining an optimal solution.

V. Conclusions

In this work, a variable-fidelity lower confidence bounding (VF-LCB) approach is proposed. In the proposed approach, a novel weighting scheme, which fully uses the local optimum distribution and global accuracy of the VF metamodel, is introduced to objectively balance global exploration and local exploitation in the determination of new sample location. Moreover, a VF-LCB sampling criterion is developed to determine the locations of new samples and the fidelity level. The VF-LCB approach is further extended to handle constraint optimization problems by introducing the probability of satisfying the constraints.

To demonstrate the efficiency and robustness of the proposed VF-LCB approach, eight numerical cases and one engineering design problem are tested. The observations are summarized: 1) For the numerical examples, the proposed VF-LCB approach can obtain an accurate global optimum with an average cost savings of about 25% compared with the other existing popular approaches. It should be noticed that, for the design of the micro-aerial vehicle problem, the average cost savings associated with the proposed VF-LCB approach are about 45% compared with the other five existing methods, while it brings about 1% increase in the weight. 2) The proposed VF-LCB approach shows obvious advantages in the robustness compared with the other compared approaches in the numerical cases. In conclusion, the VF-LCB approach can objectively balance global exploration and local exploitation to find the global optimum with high computational efficiency and robustness. In this work, genetic algorithm (GA) is used to obtain the optimum of the VF-LCB function; some other optimizers, for example, particle swarm optimization, can also be employed instead of GA. Because the VF-LCB function generally has multiple peaks, the gradient-based optimizer is difficult to get the global optimum. Practical engineering design problems always involve uncertainties, and as a part of future work, extending the proposed approach for addressing robust optimization problems will be beneficial to broaden the applicability of the approach.

Appendix A: Expression About Eight Analytical Examples

Case 1 (Forrester 1)

$$\begin{aligned} f(x) &= (6x-2)^2\sin(12x-4)\\ y_h &= f(x)\\ y_l &= 0.5f(x)+10(x-0.5)-5\\ x &\in [0,1]\\ x^* &= 0.75725, \qquad f^* = -6.020740 \end{aligned} \tag{A1}$$

Case 2

$$\begin{aligned} f(x) &= (6x-2)^2\sin(12x-4)\\ y_h &= f(x)\\ y_l &= f(x)-5\\ x &\in [0,1]\\ x^* &= 0.75725, \qquad f^* = -6.020740 \end{aligned} \tag{A2}$$

Case 3

$$f(x) = (6x-2)^2\sin(12x-4) \quad y_h = f(x) \quad y_l = f(x+0.2)$$
$$x \in [0,1] \quad x^* = 0.75725, \qquad f^* = -6.020740 \tag{A3}$$

Case 4 (Hartmann 3)

$$f(x_1,x_2,x_3) = -\sum_{i=1}^{4} c_i \exp\left[-\sum_{j=1}^{3}\alpha_{ij}(x_j-p_{ij})^2\right]$$

$$[\alpha_{ij}] = \begin{bmatrix} 3 & 10 & 30\\ 0.1 & 10 & 35\\ 3 & 10 & 30\\ 0.1 & 10 & 35 \end{bmatrix}, \quad [c_i] = \begin{bmatrix} 1\\ 1.2\\ 3\\ 3.2 \end{bmatrix},$$

$$[p_{ij}] = \begin{bmatrix} 0.3689 & 0.1170 & 0.2673\\ 0.4699 & 0.4387 & 0.7470\\ 0.1091 & 0.8732 & 0.5547\\ 0.0381 & 0.5743 & 0.8828 \end{bmatrix} \quad y_h = f(x_1,x_2,x_3)$$

$$\begin{aligned} y_l = {} & 0.585 - 0.324x_1 - 0.379x_2 - 0.431x_3 - 0.208x_1x_2\\ & + 0.326x_1x_3 + 0.193x_2x_3 + 0.225x_1^2 + 0.263x_2^2 + 0.274x_3^2 \end{aligned}$$
$$x_1,x_2,x_3 \in [0,1] \quad \boldsymbol{x}^* = (0.114, 0.556, 0.852), \; f^* = -3.8627 \tag{A4}$$

Case 5 (Ackley 5)

$$f(x_1,\ldots,x_5) = -a\exp\left[-b\sqrt{\frac{1}{n}\sum_{i=1}^{5}x_i^2}\right] - \exp\left[\frac{1}{n}\sum_{i=1}^{5}\cos(cx_i)\right] + a + \exp(1)$$
$$a = 20; \quad b = 0.2; \quad c = 2\pi \quad x_i \in [-2,2], \; i = 1,2,3,4,5$$
$$y_h = f(x_1,\ldots,x_5) \quad y_l = f(x_1,\ldots,x_5) + \sum_{i=1}^{5}x_i - \exp(1) + \exp(1.1)$$
$$\boldsymbol{x}^* = (0,\ldots,0), \quad f^* = 0.0 \tag{A5}$$

Case 6 (Hartmann 6)

$$f(x_1,\ldots,x_6) = -\sum_{i=1}^{4} c_i \exp\left[-\sum_{j=1}^{6}\alpha_{ij}(x_j-p_{ij})^2\right]$$

$$[\alpha_{ij}] = \begin{bmatrix} 10 & 3 & 17 & 3.50 & 1.7 & 8\\ 0.05 & 10 & 17 & 0.1 & 8 & 14\\ 3 & 3.5 & 1.7 & 10 & 17 & 8\\ 17 & 8 & 0.05 & 10 & 0.1 & 14 \end{bmatrix}, \quad [c_i] = \begin{bmatrix} 1.0\\ 1.2\\ 3.0\\ 3.2 \end{bmatrix}$$

$$[p_{ij}] = \begin{bmatrix} 0.1312 & 0.1696 & 0.5569 & 0.0124 & 0.8283 & 0.5886\\ 0.2329 & 0.4135 & 0.8307 & 0.3726 & 0.1004 & 0.9991\\ 0.2348 & 0.1451 & 0.3522 & 0.2883 & 0.3047 & 0.6650\\ 0.4047 & 0.8828 & 0.8732 & 0.5743 & 0.1091 & 0.0381 \end{bmatrix}$$

$$y_h = f(x_1,\ldots,x_6) \quad y_l = -\sum_{i=1}^{4} l c_i \exp\left[-\sum_{j=1}^{6}\alpha_{ij}(l_j x_j - p_{ij})^2\right]$$

$$[c_i] = \begin{bmatrix} 1.1 & 0.8 & 2.5 & 3 \end{bmatrix}^T,$$

$$[l_j] = \begin{bmatrix} 0.75 & 1 & 0.8 & 1.3 & 0.7 & 1.1 \end{bmatrix}^T \quad x_j \in [0,1],$$

$$j = 1,2,3,4,5,6$$

$$\boldsymbol{x}^* = (0.202, 0.150, 0.477, 0.275, 0.312, 0.657), \; f^* = -3.32237 \tag{A6}$$

Case 7 (Gano 2)

$$f(x_1,x_2)=4x_1^2+x_2^3+x_1x_2 \quad g(x_1,x_2)=1/x_1+1/x_2-2$$
$$y_h=f(x_1,x_2),\ g_h=g(x_1,x_2)$$
$$y_l=f(x_1+0.1,x_2-0.1)+0.1$$
$$g_l=g(x_1,x_2+0.1)-0.001 \quad x_1,x_2\in[0.1,10]$$
$$\boldsymbol{x}^*=(0.8846146,1.1500039), \qquad f^*=5.668365 \tag{A7}$$

Case 8 (G4)

$$f(x_1,\ldots,x_5)=5.3578547x_3^2+0.8356891x_1x_5+37.293239x_1-40792.141$$
$$g_1(x)=u(x)-92 \quad g_2(x)=-u(x) \quad g_3(x)=v(x)-110$$
$$g_4(x)=-v(x)+90 \quad g_5(x)=w(x)-25 \quad g_6(x)=-w(x)+20$$
$$\text{where } u(x)=85.334407+0.0056858x_2x_5+0.0006262x_1x_4-0.0022053x_3x_5$$
$$v(x)=80.51249+0.0071317x_2x_5+0.0029955x_1x_2+0.002183x_3^2$$
$$w(x)=9.300961+0.0047026x_3x_5+0.0012547x_1x_3+0.0012085x_3x_4$$
$$y_h=f(x_1,\ldots,x_5),\ u_h(x)=u(x),\ v_h(x)=v(x),\ w_h(x)=w(x)$$
$$y_l=5.3578547(x_3+0.1)^2+0.8356891(x_1-5)(x_5+1)+37.293239(x_1-5)+3.511348x_2x_4-30792.141$$
$$u_l(x)=84.334407+0.0066858(x_2+1)(x_5-1)+0.0016262x_1x_4-0.0042053x_3(x_5-1)$$
$$v_l(x)=81.51249+0.0061317(x_2+1)(x_5-1)+0.0129955x_1(x_2+1)+0.001183x_3^2$$
$$w_l(x)=10.300961+0.0027026x_3(x_5-1)+0.0012547x_1x_3+0.0009085x_3x_4$$
$$x_1\in[78,102],\quad x_2\in[33,45],\quad x_i\in[27,45],\quad i=3,4,5$$
$$\boldsymbol{x}^*=(78,33,29.99525,45,36.77581),\ f^*=-30{,}665.539 \tag{A8}$$

Appendix B: Details of the Compared Methods

B.1. Standard Expected Improvement Method

For the prediction of the kriging model, an untried point can be regarded as a random variable of a normal distribution $Y\sim N(\hat{y}(\boldsymbol{x}),s(\boldsymbol{x}))$, which has mean $\hat{y}(\boldsymbol{x})$ and standard deviation $s(\boldsymbol{x})$. The statistical improvement of the prediction with respect to the current optimum is defined as,

$$I(\boldsymbol{x})=\max(y_{\min}-Y,0) \tag{B1}$$

EI is the expectation of this improvement, and it can be written as,

$$E[I(\boldsymbol{x})]=\begin{cases}(f_{\min}-\hat{y})\Phi\left(\frac{f_{\min}-\hat{y}(\boldsymbol{x})}{s(\boldsymbol{x})}\right)+s\phi\left(\frac{f_{\min}-\hat{y}(\boldsymbol{x})}{s(\boldsymbol{x})}\right) & \text{if } s(\boldsymbol{x})>0\\ 0 & \text{if } s(\boldsymbol{x})=0\end{cases} \tag{B2}$$

where $\phi(\cdot)$ and $\Phi(\cdot)$ are the standard normal density and distribution function, respectively, and $\hat{y}(\boldsymbol{x})$ and $s(\boldsymbol{x})$ denote predicted value and standard error at the point $\boldsymbol{x}$, respectively.

For a constrained optimization problem, the probability of feasible for each constrain is evaluated by Eq. (19), and the constrained EI function is formulated as,

$$\mathrm{CEI}(x)=\mathrm{EI}(x)\cdot\prod_{i=1}^{N_c}P[G_i(\boldsymbol{x},t)\le 0] \tag{B3}$$

where N_c represents the number of constrains, and G_i denotes the prediction of the ith constrained model.

B.2. Augmented Expected Improvement Function

The AEI function adopts a Bayesian point of view on kriging metamodeling for an intuitive presentation of the EI function, which was proposed by Huang et al. in their MFSKO method. The AEI function can be expressed as,

$$\mathrm{EI}(\boldsymbol{x},l)=E[\max(\hat{f}_m(\boldsymbol{x}^*)-f_m^p(\boldsymbol{x}),0)]\cdot\alpha_1(\boldsymbol{x},l)\cdot\alpha_2(\boldsymbol{x},l)\cdot\alpha_3(l) \tag{B4}$$

The four product terms to the right of the equation can be calculated analytically as,

$$E[\max(\hat{f}_m(\boldsymbol{x}^*)-f_m^p(\boldsymbol{x}),0)]=(\hat{f}_m(\boldsymbol{x}^*)-\hat{f}_m(\boldsymbol{x}))\Phi\left(\frac{\hat{f}_m(\boldsymbol{x}^*)-\hat{f}_m(\boldsymbol{x})}{s_m(\boldsymbol{x})}\right)+s_m(\boldsymbol{x})\phi\left(\frac{\hat{f}_m(\boldsymbol{x}^*)-\hat{f}_m(\boldsymbol{x})}{s_m(\boldsymbol{x})}\right) \tag{B5}$$

$$\alpha_1(\boldsymbol{x},l)=\mathrm{corr}[f_l^p(\boldsymbol{x}),f_m^p(\boldsymbol{x})] \tag{B6}$$

$$\alpha_2(\boldsymbol{x},l)=\left(1-\frac{\sigma_{\varepsilon,l}}{\sqrt{s_l^2(\boldsymbol{x})+\sigma_{\varepsilon,l}^2}}\right) \tag{B7}$$

$$\alpha_3(l)=\frac{C_m}{C_l} \tag{B8}$$

where l denotes the fidelity level, m represents the highest-fidelity level, and $\boldsymbol{x}^*$ stands for the current effective best solution. $\alpha_2(\boldsymbol{x},l)$ is the consideration of random errors ε. $\alpha_3(l)$ is the ratio between the cost per evaluation on the highest-fidelity system m and the system l, and corr stands for correlation and it can be calculated as,

$$\mathrm{cov}[f_l^p(\boldsymbol{x}),f_m^p(\boldsymbol{x}')]=\mathrm{cov}[f_l(\boldsymbol{x}),f_m(\boldsymbol{x}')]-[\boldsymbol{h}_l(\boldsymbol{x})^T,\boldsymbol{r}_l(\boldsymbol{x})^T]\begin{bmatrix}0 & \boldsymbol{P}^T\\ \boldsymbol{P} & \boldsymbol{R}\end{bmatrix}^{-1}\begin{bmatrix}\boldsymbol{h}_m(\boldsymbol{x}')\\ \boldsymbol{r}_m(\boldsymbol{x}')\end{bmatrix} \tag{B9}$$

where $\boldsymbol{P}$, $\boldsymbol{R}$, $\boldsymbol{h}$, and $\boldsymbol{r}$ are expressed in Eq. (3).

B.3. Variable-Fidelity Expected Improvement Method

The VF-EI method employs HK to analytically formulate the expected improvement function associated with a lower-fidelity model. Similar to the standard EI function, the VF-EI is derived as,

$$\mathrm{EI}_{\mathrm{vf}}(\boldsymbol{x},l)=\begin{cases}(y_{\min}-\hat{y}(\boldsymbol{x}))\Phi\left(\frac{y_{\min}-\hat{y}(\boldsymbol{x})}{s(\boldsymbol{x},l)}\right)+s(\boldsymbol{x},l)\phi\left(\frac{y_{\min}-\hat{y}(\boldsymbol{x})}{s(\boldsymbol{x},l)}\right), & \text{if } s(\boldsymbol{x},l)>0\\ 0, & \text{if } s(\boldsymbol{x},l)=0\end{cases} \tag{B10}$$

where the model uncertainty of the HK model is calculated by,

$$s^2(x,l)=\begin{cases}\beta_0^2 s_{lf}^2(x) & l=1 \text{ for LF level}\\ s^2(x) & l=2 \text{ for HF level}\end{cases} \tag{B11}$$

where β_0^2 is the scaling factor in the HK model, and $s^2(x)$ is the uncertainty of the HK model.

B.4. Multifidelity Optimization Using Statistical Surrogate Method

The MFO method considers a second information source (IS) of uncertainty to be inherent to the IS itself. Combing the uncertainty stemming from the fidelity of the IS and the uncertainty in the Gaussian process, the total variance is defined by,

$$\sigma_{t,m}^2 = \sigma_{GP,m}^2(\boldsymbol{x}) + \sigma_{f,m}^2(\boldsymbol{x}) \tag{B12}$$

where $\sigma_{GP,m}^2(\boldsymbol{x})$ and $\sigma_{f,m}^2(\boldsymbol{x})$ are, respectively, the variance associated with the Gaussian process and the fidelity variance of IS f_m.

By constructing each IS surrogate, respectively, the multifidelity surrogate can be obtained as,

$$S_X \sim N(\bar{\mu}(\boldsymbol{x}), \bar{\sigma}(\boldsymbol{x})) \tag{B13}$$

$$\bar{\sigma}^2(\boldsymbol{x}) = \left(\sum_{m=1}^{M} \frac{1}{\sigma_{t,m}^2(\boldsymbol{x})}\right)^{-1} \tag{B14}$$

$$\bar{\mu}(\boldsymbol{x}) = \bar{\sigma}^2(\boldsymbol{x}) \sum_{m=1}^{M} \frac{\mu(\boldsymbol{x})}{\sigma_{t,m}^2(\boldsymbol{x})} \tag{B15}$$

where $\mu(\boldsymbol{x})$ is the approximate estimation of the mth surrogate model.

An extension of EI function is taken to choose a new design point according to the multifidelity surrogate, and the extended EI function can be expressed as,

$$\mathrm{EI}_{MF}(\boldsymbol{x}) = (y_{\min} - \bar{\mu}(\boldsymbol{x}))\Phi\left(\frac{y_{\min} - \bar{\mu}(\boldsymbol{x})}{\hat{\sigma}(\boldsymbol{x})}\right) + \hat{\sigma}(\boldsymbol{x})\phi\left(\frac{y_{\min} - \bar{\mu}(\boldsymbol{x})}{\hat{\sigma}(\boldsymbol{x})}\right) \tag{B16}$$

$$\hat{\sigma}(\boldsymbol{x}) = \left(\sum_{m=1}^{M} \frac{1}{\sigma_{GP,m}^2(\boldsymbol{x})}\right)^{-1} \tag{B17}$$

when the maximum EI found is lower than a threshold ε_{ei}, a strategy of minimizing the multifidelity surrogate estimation is substituted,

$$\boldsymbol{x}_{n+1} = \arg\ \min \bar{\mu}(\boldsymbol{x}) \tag{B18}$$

Acknowledgments

This research has been supported by the National Natural Science Foundation of China (NSFC) under Grant Nos. 51805179, 51775203, and 51721092, and the Fundamental Research Funds for the Central Universities (HUST; Grant No. 2016YXMS272). The authors would also like to thank the anonymous referees for their valuable comments.

References

[1] Wang, Z., and Ierapetritou, M., "Constrained Optimization of Black-Box Stochastic Systems Using a Novel Feasibility Enhanced Kriging-Based Method," *Computers & Chemical Engineering*, Vol. 118, Oct. 2018, pp. 210–223. doi:10.1016/j.compchemeng.2018.07.016

[2] Liu, H., Xu, S., Wang, X., Meng, J., and Yang, S., "Optimal Weighted Pointwise Ensemble of Radial Basis Functions with Different Basis Functions," *AIAA Journal*, Vol. 54, No. 10, 2016, pp. 3117–3133. doi:10.2514/1.j054664

[3] Han, Z.-H., Chen, J., Zhang, K.-S., Xu, Z.-M., Zhu, Z., and Song, W.-P., "Aerodynamic Shape Optimization of Natural-Laminar-Flow Wing Using Surrogate-Based Approach," *AIAA Journal*, Vol. 56, No. 7, 2018, pp. 2579–2593. doi:10.2514/1.J056661

[4] Zhang, K.-S., Han, Z.-H., Gao, Z.-J., and Wang, Y., "Constraint Aggregation for Large Number of Constraints in Wing Surrogate-Based Optimization," *Structural and Multidisciplinary Optimization*, Vol. 59, No. 2, 2019, pp. 421–438. doi:10.1007/s00158-018-2074-4

[5] Hawchar, L., El Soueidy, C.-P., and Schoefs, F., "Principal Component Analysis and Polynomial Chaos Expansion for Time-Variant Reliability Problems," *Reliability Engineering & System Safety*, Vol. 167, Nov. 2017, pp. 406–416. doi:10.1016/j.ress.2017.06.024

[6] Chatterjee, T., Chakraborty, S., and Chowdhury, R., "A Critical Review of Surrogate Assisted Robust Design Optimization," *Archives of Computational Methods in Engineering*, Vol. 26, No. 1, 2019, pp. 245–274.

[7] Zhou, Q., Jiang, P., Shao, X., Hu, J., Cao, L., and Wan, L., "A Variable Fidelity Information Fusion Method Based on Radial Basis Function," *Advanced Engineering Informatics*, Vol. 32, April 2017, pp. 26–39. doi:10.1016/j.aei.2016.12.005

[8] Shi, R., Liu, L., Long, T., and Liu, J., "Sequential Radial Basis Function Using Support Vector Machine for Expensive Design Optimization," *AIAA Journal*, Vol. 55, No. 1, 2017, pp. 214–227. doi:10.2514/1.J054832

[9] Liu, H., Ong, Y.-S., Cai, J., and Wang, Y., "Cope with Diverse Data Structures in Multi-Fidelity Modeling: A Gaussian Process Method," *Engineering Applications of Artificial Intelligence*, Vol. 67, Jan. 2018, pp. 211–225. doi:10.1016/j.engappai.2017.10.008

[10] Han, Z.-H., Zhang, Y., Song, C.-X., and Zhang, K.-S., "Weighted Gradient-Enhanced Kriging for High-Dimensional Surrogate Modeling and Design Optimization," *AIAA Journal*, Vol. 55, No. 12, 2017, pp. 4330–4346. doi:10.2514/1.J055842

[11] Zhou, Q., Shao, X., Jiang, P., Zhou, H., and Shu, L., "An Adaptive Global Variable Fidelity Metamodeling Strategy Using a Support Vector Regression Based Scaling Function," *Simulation Modelling Practice and Theory*, Vol. 59, Dec. 2015, pp. 18–35. doi:10.1016/j.simpat.2015.08.002

[12] Xie, T., Jiang, P., Zhou, Q., Shu, L., Zhang, Y., Meng, X., and Wei, H., "Advanced Multi-Objective Robust Optimization Under Interval Uncertainty Using Kriging Model and Support Vector Machine," *Journal of Computing and Information Science in Engineering*, Vol. 18, No. 4, 2018, Paper 041012. doi:10.1115/1.4040710

[13] Patterson, D. W., *Artificial Neural Networks: Theory and Applications*, Prentice Hall PTR, 1998, pp. 1–400.

[14] Villarrubia, G., De Paz, J. F., Chamoso, P., and De la Prieta, F., "Artificial Neural Networks Used in Optimization Problems," *Neurocomputing*, Vol. 272, Jan. 2018, pp. 10–16. doi:10.1016/j.neucom.2017.04.075

[15] Zhou, Q., Shao, X., Jiang, P., Gao, Z., Wang, C., and Shu, L., "An Active Learning Metamodeling Approach by Sequentially Exploiting Difference Information from Variable-Fidelity Models," *Advanced Engineering Informatics*, Vol. 30, No. 3, 2016, pp. 283–297. doi:10.1016/j.aei.2016.04.004

[16] Rumpfkeil, M. P., and Beran, P., "Construction of Dynamic Multifidelity Locally Optimized Surrogate Models," *AIAA Journal*, Vol. 59, No. 9, 2017, pp. 1–11. doi:10.2514/1.j055834

[17] Cai, X., Qiu, H., Gao, L., Wei, L., and Shao, X., "Adaptive Radial-Basis-Function-Based Multifidelity Metamodeling for Expensive Black-Box Problems," *AIAA Journal*, Vol. 55, No. 7, 2017, pp. 2424–2436. doi:10.2514/1.J055649

[18] Viana, F. A. C., Simpson, T. W., Balabanov, V., and Toropov, V., "Special Section on Multidisciplinary Design Optimization: Metamodeling in Multidisciplinary Design Optimization: How Far Have We Really Come?" *AIAA Journal*, Vol. 52, No. 4, 2014, pp. 670–690. doi:10.2514/1.J052375

[19] Chen, S., Jiang, Z., Yang, S., and Chen, W., "Multimodel Fusion Based Sequential Optimization," *AIAA Journal*, Vol. 55, No. 1, 2016, pp. 1–14. doi:10.2514/1.j054729

[20] Gano, S. E., Renaud, J. E., and Sanders, B., "Hybrid Variable Fidelity Optimization by Using a Kriging-Based Scaling Function," *AIAA Journal*, Vol. 43, No. 11, 2005, pp. 2422–2433. doi:10.2514/1.12466

[21] Haftka, R. T., "Combining Global and Local Approximations," *AIAA Journal*, Vol. 29, No. 9, 1991, pp. 1523–1525. doi:10.2514/3.10768

[22] Lewis, R., and Nash, S., "A Multigrid Approach to the Optimization of Systems Governed by Differential Equations," *8th Symposium on Multidisciplinary Analysis and Optimization*, AIAA Paper 2000-4890, 2000.

[23] Park, C., Haftka, R. T., and Kim, N. H., "Remarks on Multi-Fidelity Surrogates," *Structural and Multidisciplinary Optimization*, Vol. 55,

No. 3, 2017, pp. 1029–1050.
doi:10.1007/s00158-016-1550-y
[24] Bakr, M. H., Bandler, J. W., Madsen, K., and Søndergaard, J., "An Introduction to the Space Mapping Technique," *Optimization and Engineering*, Vol. 2, No. 4, 2001, pp. 369–384.
doi:10.1023/A:1016086220943
[25] Leifsson, L., Koziel, S., and Tesfahunegn, Y. A., "Multiobjective Aerodynamic Optimization by Variable-Fidelity Models and Response Surface Surrogates," *AIAA Journal*, Vol. 54, No. 2, 2016, pp. 531–541.
doi:10.2514/1.J054128
[26] Xiao, M., Zhang, G., Breitkopf, P., Villon, P., and Zhang, W., "Extended Co-Kriging Interpolation Method Based on Multi-Fidelity Data," *Applied Mathematics and Computation*, Vol. 323, April 2018, pp. 120–131.
doi:10.1016/j.amc.2017.10.055
[27] Kennedy, M. C., and O'Hagan, A., "Predicting the Output from a Complex Computer Code When Fast Approximations Are Available," *Biometrika*, Vol. 87, No. 1, 2000, pp. 1–13.
doi:10.1093/biomet/87.1.1
[28] Han, Z.-H., and Görtz, S., "Hierarchical Kriging Model for Variable-Fidelity Surrogate Modeling," *AIAA Journal*, Vol. 50, No. 9, 2012, pp. 1885–1896.
doi:10.2514/1.J051354
[29] Shan, S., and Wang, G. G., "Survey of Modeling and Optimization Strategies to Solve High-Dimensional Design Problems with Computationally-Expensive Black-Box Functions," *Structural and Multidisciplinary Optimization*, Vol. 41, No. 2, 2010, pp. 219–241.
doi:10.1007/s00158-009-0420-2
[30] Qian, J., Yi, J., Cheng, Y., Liu, J., and Zhou, Q., "A Sequential Constraints Updating Approach for Kriging Surrogate Model-Assisted Engineering Optimization Design Problem," *Engineering with Computers*, 2019, pp. 1–17.
[31] Jones, D. R., Schonlau, M., and Welch, W. J., "Efficient Global Optimization of Expensive Black-Box Functions," *Journal of Global Optimization*, Vol. 13, No. 4, 1998, pp. 455–492.
doi:10.1023/A:1008306431147
[32] Cox, D. D., and John, S., "A Statistical Method for Global Optimization," *[Proceedings] 1992 IEEE International Conference on Systems, Man, and Cybernetics*, IEEE, New York, 1992, pp. 1241–1246.
[33] Li, Y., Wu, Y., Zhao, J., and Chen, L., "A Kriging-Based Constrained Global Optimization Algorithm for Expensive Black-Box Functions with Infeasible Initial Points," *Journal of Global Optimization*, Vol. 67, Nos. 1–2, 2017, pp. 343–366.
doi:10.1007/s10898-016-0455-z
[34] Cheng, J., Jiang, P., Zhou, Q., Jiexiang, H., Tao, Y., Leshi, S., and Xinyu, S., "A Lower Confidence Bounding Approach Based on the Coefficient of Variation for Expensive Global Design Optimization," *Engineering Computations*, Vol. 36 No. 3, 2019, pp. 830–849.
[35] Dong, H., Song, B., Wang, P., and Dong, Z., "Hybrid Surrogate-Based Optimization Using Space Reduction (HSOSR) for Expensive Black-Box Functions," *Applied Soft Computing*, Vol. 64, March 2018, pp. 641–655.
doi:10.1016/j.asoc.2017.12.046
[36] Qin, C., Klabjan, D., and Russo, D., "Improving the Expected Improvement Algorithm," *Advances in Neural Information Processing Systems*, Long Beach Convention Center, Long Beach, CA, Neural Information Processing Systems (NIPS), 2017, pp. 5381–5391.
[37] Zheng, J., Li, Z., Gao, L., and Jiang, G., "A Parameterized Lower Confidence Bounding Scheme for Adaptive Metamodel-Based Design Optimization," *Engineering Computations*, Vol. 33, No. 7, 2016, pp. 2165–2184.
doi:10.1108/EC-04-2015-0088
[38] Song, X., Lv, L., Li, J., Sun, W., and Zhang, J., "An Advanced and Robust Ensemble Surrogate Model: Extended Adaptive Hybrid Functions," *Journal of Mechanical Design*, Vol. 140, No. 4, 2018, Paper 041402.
doi:10.1115/1.4039128
[39] Li, E., and Wang, H., "An Alternative Adaptive Differential Evolutionary Algorithm Assisted by Expected Improvement Criterion and Cut-HDMR Expansion and its Application in Time-Based Sheet Forming Design," *Advances in Engineering Software*, Vol. 97, July 2016, pp. 96–107.
doi:10.1016/j.advengsoft.2016.03.001
[40] Huang, D., Allen, T. T., Notz, W. I., and Miller, R. A., "Sequential Kriging Optimization Using Multiple-Fidelity Evaluations," *Structural and Multidisciplinary Optimization*, Vol. 32, No. 5, 2006, pp. 369–382.
doi:10.1007/s00158-005-0587-0
[41] Xiong, Y., Chen, W., and Tsui, K.-L., "A New Variable-Fidelity Optimization Framework Based on Model Fusion and Objective-Oriented Sequential Sampling," *Journal of Mechanical Design*, Vol. 130, No. 11, 2008, Paper 111401.
doi:10.1115/1.2976449
[42] Zhang, Y., Han, Z.-H., and Zhang, K.-S., "Variable-Fidelity Expected Improvement Method for Efficient Global Optimization of Expensive Functions," *Structural and Multidisciplinary Optimization*, Vol. 58, No. 4, 2018, pp. 1431–1451.
doi:10.1007/s00158-018-1971-x
[43] Liu, Y., Chen, S., Wang, F., and Xiong, F., "Sequential Optimization Using Multi-Level Cokriging and Extended Expected Improvement Criterion," *Structural and Multidisciplinary Optimization*, Vol. 58, No. 3, 2018, pp. 1155–1173.
doi:10.1007/s00158-018-1959-6
[44] Sacks, J., Welch, W. J., Mitchell, T. J., and Wynn, H. P., "Design and Analysis of Computer Experiments," *Statistical Science*, Vol. 4, No. 4, 1989, pp. 409–423.
doi:10.1214/ss/1177012413
[45] Zhang, Y., Kim, N. H., Park, C., and Haftka, R. T., "Multifidelity Surrogate Based on Single Linear Regression," *AIAA Journal*, Vol. 56, No. 12, 2018, pp. 4944–4952.
doi:10.2514/1.J057299
[46] Yamazaki, W., and Mavriplis, D. J., "Derivative-Enhanced Variable Fidelity Surrogate Modeling for Aerodynamic Functions," *AIAA Journal*, Vol. 51, No. 1, 2013, pp. 126–137.
doi:10.2514/1.J051633
[47] Zadeh, P. M., Toropov, V. V., and Wood, A. S., "Metamodel-Based Collaborative Optimization Framework," *Structural and Multidisciplinary Optimization*, Vol. 38, No. 2, 2009, pp. 103–115.
doi:10.1007/s00158-008-0286-8
[48] Robinson, T., Eldred, M., Willcox, K., and Haimes, R., "Surrogate-Based Optimization Using Multifidelity Models with Variable Parameterization and Corrected Space Mapping," *AIAA Journal*, Vol. 46, No. 11, 2008, pp. 2814–2822.
doi:10.2514/1.36043
[49] Shu, L., Jiang, P., Zhou, Q., Shao, X., Hu, J., and Meng, X., "An On-Line Variable Fidelity Metamodel Assisted Multi-Objective Genetic Algorithm for Engineering Design Optimization," *Applied Soft Computing*, Vol. 66, May 2018, pp. 438–448.
doi:10.1016/j.asoc.2018.02.033
[50] Coello, C. A. C., "Use of a Self-Adaptive Penalty Approach for Engineering Optimization Problems," *Computers in Industry*, Vol. 41, No. 2, 2000, pp. 113–127.
doi:10.1016/S0166-3615(99)00046-9
[51] Lam, R., Allaire, D. L., and Willcox, K. E., "Multifidelity Optimization Using Statistical Surrogate Modeling for Non-Hierarchical Information Sources," *56th AIAA/ASCE/AHS/ASC Structures, Structural Dynamics, and Materials Conference*, AIAA Paper 2015-0143, 2015.
[52] Forrester, A. I., Sóbester, A., and Keane, A. J., "Multi-Fidelity Optimization via Surrogate Modelling," *Proceedings of the Royal Society of London A: Mathematical, Physical and Engineering Sciences*, Vol. 463, No. 2088, 2007, pp. 3251–3269.
[53] Hartman, J. K., "Some Experiments in Global Optimization," *Naval Research Logistics Quarterly*, Vol. 20, No. 3, 1973, pp. 569–576.
doi:10.1002/(ISSN)1931-9193
[54] Hedar, A.-R., and Ahmed, A., "Studies on Metaheuristics for Continuous Global Optimization Problems," Ph.D. Thesis, Kyoto Univ., Kyoto, Japan, 2004.
[55] Ackley, D. H., "The Model," *A Connectionist Machine for Genetic Hillclimbing*, Kluwer, Dordrecht, The Netherlands, 1987, pp. 29–70.
[56] Garcia, S., and Herrera, F., "An Extension on 'Statistical Comparisons of Classifiers over Multiple Data Sets' for All Pairwise Comparisons," *Journal of Machine Learning Research*, Vol. 9, Dec. 2008, pp. 2677–2694.
[57] Friedman, M., "The Use of Ranks to Avoid the Assumption of Normality Implicit in the Analysis of Variance," *Journal of the American Statistical Association*, Vol. 32, No. 200, 1937, pp. 675–701.
doi:10.1080/01621459.1937.10503522
[58] Bergmann, B., and Hommel, G., "Improvements of General Multiple Test Procedures for Redundant Systems of Hypotheses," *Multiple Hypothesenprüfung/Multiple Hypotheses Testing*, Springer, Berlin, Heidelberg, 1988, pp. 100–115.
[59] Nguyen, J., Park, S.-I., and Rosen, D., "Heuristic Optimization Method for Cellular Structure Design of Light Weight Components," *International Journal of Precision Engineering and Manufacturing*, Vol. 14, No. 6, 2013, pp. 1071–1078.
doi:10.1007/s12541-013-0144-5

F. Grasso
Associate Editor